Metallic Fuels

Gerard L. Hofman
University of Chicago, Argonne National Laboratory, 9700 South Cass Avenue, Argonne, IL 60439-4820 USA

List of Symbols

D	Diffusivity
D_i	Diffusivity of the migrating solute (component i of a homogeneous solution)
ΔH_i	Partial molar enthalpy of solution for component i
J_i	Solute flux of component i in a homogeneous solution
N_i	Concentration of the migrating solute (component i of a homogeneous solution)
P_i	Internal gas pressure
P_ex	External pressure
Q^*	Heat of transport
Q_e, Q_p	Component of Q^* attributed to the electron, phonon "wind"

Materials Science and Technology,

Q_{in}	Intrinsic component of Q^*
R	Bubble radius, gas content
T	Temperature
Γ	Bubble surface tension

List of Abbreviations

ANL	Argonne National Laboratory
BOL	Beginning of life
BU	Burnup
CP-5	Chicago pile no. 5 reactor
DFR	Dounreay fast reactor
DN	Delayed neutron
DPH	Diamond pyramid hardness
EBR-I, II	Experimental breeder reactor I, II
FCCI	Fuel–cladding chemical interaction
FCMI	Fuel–cladding mechanical interaction
FPIN2	Fuel behavior modeling code (transient) (ANL)
Hex	Hexagonal
IFR	Integral fast reactor
LIFE-METAL	Fuel behavior modeling code (ANL)
LMR	Liquid-metal-cooled fast reactor
MK-IA, II	EBR-II fuel element type IA, II
RBCB	Run beyond cladding breach
SEM	Scanning electron microscopy
TEM	Transmission electron microscopy
TOP	Transient overpower
TREAT	Transient reactor test facility

1 Introduction

This chapter describes the irradiation behavior of the first fuels to be used in nuclear reactors – the metals U, Pu, and Th, and their alloys. Starting in the late 1940s, metallic fuels dominated the early development of nuclear reactors because of their key attributes of high fissile-atom density and good thermal conductivity. Although Th has a relatively low density, it is always used in combination with either U and/or Pu and imparts a high thermal conductivity for all fuel combinations (Fig. 1). And yet initial experiments with pure U metal met with spectacular swelling and growth (Fig. 2), as described by Paine and Kittel (1955) at the first UN Conference on Peaceful Uses of Atomic Energy, and further described by them at the second of these conferences (Kittel and Paine, 1958).[1)]

[1)] A total of four such conferences were held in 1955, 1958, 1964, and 1971. These were unique international forums that addressed all aspects of atomic energy, including advances in reactor fuels and materials.

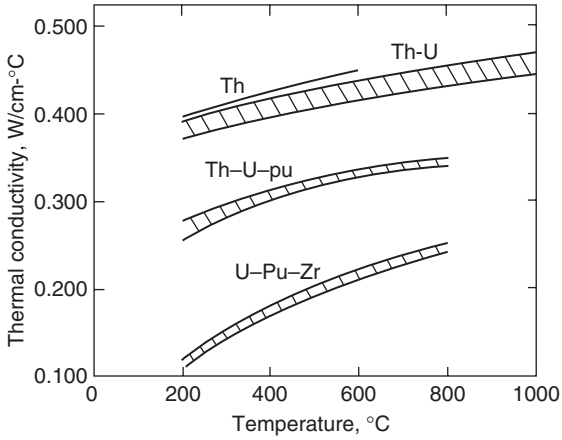

Fig. 1 Thermal conductivity of Th, and Th–U, Th–U-Pu and U–Pu–Zr alloys. After Kittel (1977).

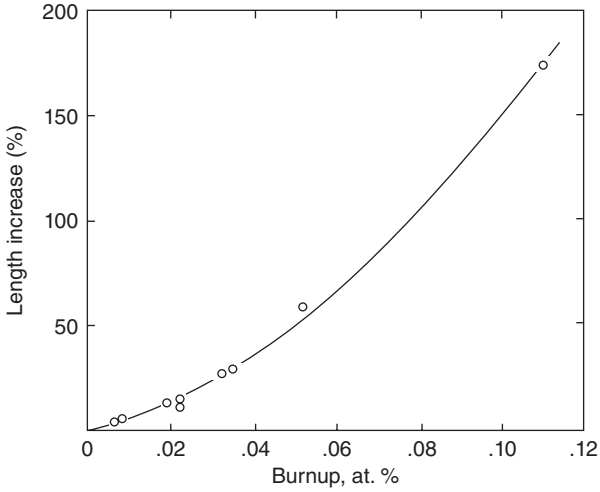

Fig. 2 Length changes in unalloyed U specimens rolled at 300 °C and irradiated in an unrestrained condition. After Kittel and Paine (1958).

Metal fuels were mainly destined for reactors that used natural U to produce Pu for military purposes. The British and French CO_2-cooled graphite-moderated production reactors generated electricity in addition to producing Pu. Through to the mid-1950s, metallurgists in the West and in Russia put a great deal of effort into removing texture, grain refining, and adding minor amounts of alloying elements in order to achieve an acceptable irradiation behavior of high-density U, albeit to low burnup. Depending on the country of origin, the resulting alloys were known as "adjusted" U, "Springfield" U,[2)] and "sicral"

[2)] Springfield U used in the UK Uranium-Magnox reactors typically contained 260 ppm Fe, 650 ppm Al, 800 ppm C, 20 ppm Si, and 50 ppm Ni (Jepson and Hindmarch, 1964).

U;[3] Russian alloys were described by Zaimovsky (1958). This busy period of development was reviewed by Pugh (1955). The fabrication methods developed for these fuels and their measured properties have been fully treated by Harrington and Ruehle (1958) and Gittus (1963), and many others, and therefore are not considered here.

The properties of metallic fuels made them attractive as fuels for fast breeder reactors, and this application was actively pursued. It became clear that, with the addition of Pu, more than minor alloying additions were required in order to obtain acceptable irradiation behaviors. The elimination of anisotropic phases was the key development, and this was accomplished by the addition of about 20 at.% of Mo, Nb, Zi, or Ti. However, the swelling behavior at high temperature did not allow burnups above ~3 at.%. The solution to this problem was to allow the fuel to swell within its cladding to the point where the majority of fission gas was released to a suitably sized plenum, as in the Experimental Breeder Reactor II (EBR-II), or directly vented to the coolant, as in the Dounreay Fast Reactor (DFR).

By the mid-1960s, designers of both large fast reactors and large gas-cooled thermal reactors had turned to the use of ceramic oxides because of their high-burnup capability, and metal fuels were no longer actively studied, except at Argonne National Laboratory (ANL). Between 1984 and 1994, however, a revival of metal fuels took place in the United States with the Integral Fast Reactor (IFR) program, and U–Pu–Zr alloys were further investigated at ANL. Section 2.6 in this chapter is devoted to IFR fuel.

[3] "Sicral" stands for Si, Cr, Al – minor alloy additions used in France.

Today, U–Pu–Zr alloys are again under study for the destruction ("burning") of the minor actinides Np, Am, and Cm, extracted from spent power reactor fuel and irradiated in advanced fast burner reactors designed for that purpose (Chang *et al.*, 2006).

Also under current development are high-density U–Mo alloys for the conversion of research and test reactors from high-enrichment U (HEU) to proliferation-resistant low-enrichment U (LEU), as discussed in Chapter Dispersion Fuels.

With regards to thorium, in spite of early positive irradiation test results on its alloys, the Th/U breeding cycle never gained sufficient interest in the West to warrant a fuel development effort. The exception to this trend was India, a country with ample Th resources and little U; even there, however, ceramic Th compounds became the preferred fuel.

2 Irradiation Behavior

2.1 Swelling and Gas Release

2.1.1 Uranium

Uranium melts at 1130 °C, has the highest density of all elements (18.96 mg m^{-3}), and the highest thermal conductivity of all fuels (27–50 W m^{-1} °C^{-1} over 0–1130 °C). Uranium has three allotropic forms: high-temperature γ-U is body-centered cubic; on cooling to 772 °C it transforms to tetragonal β-U, which in turn transforms to orthorhombic α-U at 669 °C. Fuel elements used in metal-fueled reactors operate mostly in a temperature range where α is the equilibrium phase; α-U has, therefore, been the subject of extensive study.

The most important irradiation characteristic of α-U is its dimensional instability in the form of anisotropic growth and swelling, which results from the anisotropy of the orthorhombic crystal structure (see Fig. 3) (Kulcinsky *et al.*, 1969). Anisotropic irradiation growth is defined as a change of shape without any significant increase in volume. Among others, Paine and Kittel (1955) and Loomis and Gerber (1968) have shown that single crystals of α-U elongate in the [010] direction and contract in the [100] direction, with no appreciable change along the [001] axis (see Fig. 4). The most accepted theory of this phenomenon is due to Buckley (1961, 1966), who showed that fission-generated interstitials and vacancies form loops on {010} and {110} planes, respectively, as a result of the anisotropic thermal expansion induced in α-U by thermal spikes in displacement cascades. In essence, this represents a mass transport from {110} planes to {010} planes.

Electron microscopy confirmed the existence of such loops (see Makin *et al.*, 1962 and Hudson, 1964). The temperature dependence of this growth process takes on the familiar bell-shaped form, due to interaction (recombination) of fission-produced and thermally activated point defects. In a polycrystalline sample this mass transport in individual grains results in shape changes and, thereby, in mismatched strains between the individual grains. The stress developed due to these mismatched strains can be released by plastic deformation at the grain boundaries; this is commonly referred to as tearing or cavitation. If, as a result of the fabrication techniques used, a preferred orientation or texture is present in such a polycrystal, net anisotropic strain is observed.

Swelling of uranium is governed by several mechanisms. As in other fuels, a

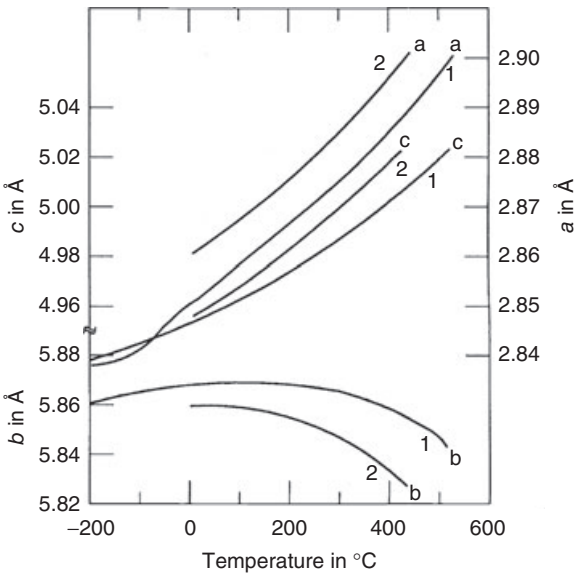

Fig. 3 Temperature dependence of axial lattice parameters of (curves 1) α-U and (curves 2) α-U-15 at.% Pu. After Kulcinsky *et al.* (1969).

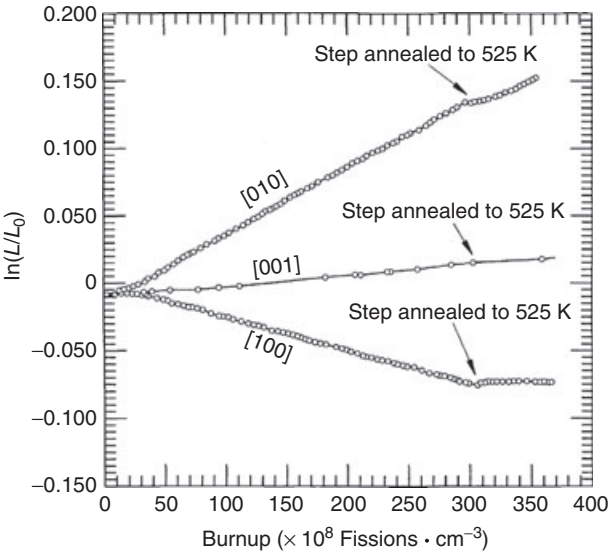

Fig. 4 Length changes in the three directions [100], [010] and [001] for a uranium single crystal irradiated at 4 K. After Loomis and Gerber (1968).

basic mechanism of accommodating solid, liquid, and gaseous fission products results in a burnup- and temperature-dependent volume increase, of a magnitude controlled by U fission-product alloy chemistry and by the precipitation and growth of Xe/Kr gas bubbles. However, between 400 and 600 °C swelling is overwhelmingly dominated by cavitation. In introducing this mechanism, Angerman and Caskey (1964) and Lehmann *et al.* (1969) showed that swelling of up to 50 vol.% could occur at burnups below 0.5 at.%.

Cavitation swelling is characterized by large irregular cavities that form by mechanical tearing at grain and sub-grain boundaries, resulting in a very deformed "swirled" microstructure, as shown in Fig. 5; see also Bellamy (1962), Leggett, Mastel, and Bierlein (1963), and Leggett, Bierlein, and Mastel (1967). In addition to these large cavities, many small cavities, or tears, develop within the α grains, particularly in the 500–600 °C range. These intergranular cavities are crystallographically aligned and appear to be related to twin boundaries (Claudson *et al.*, 1959; Mikailoff, 1964) (see Fig. 6); they probably result from dislocation interaction and vacancy condensation (Leteurtre, 1969). Because cavitational swelling is related to anisotropic growth in α-U, it is susceptible to preferred grain orientation and to the stress state existing during irradiation. It is not driven by fission gas and is basically a process that occurs at low temperature. Because tears are practically empty, cavitational swelling is relatively compressible; however, at higher burnup fission gas will collect in the preformed cavities, pressurize them, and impart bubble-like properties to them. Unless the fission gas is able to escape, the buildup of internal pressure will make the fuel less compressible.

Since cavitation appears to be caused by irradiation-induced point defects, metallurgical phenomena in the fuel that control point-defect behavior should also

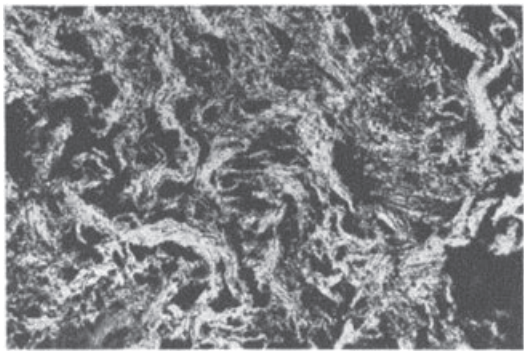

(a) Unalloyed uranium, 1250 MWD/T

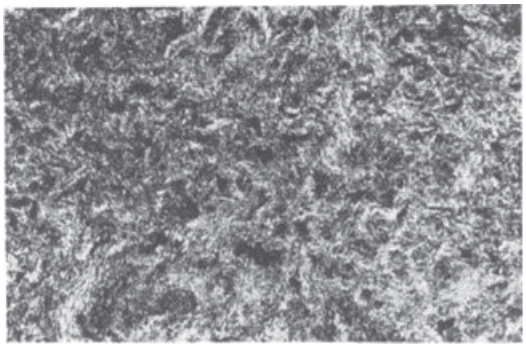

(b) U – 150 ppm Fe – 100 ppm si, 2130 MWD/T

Fig. 5 Cavities formed in (a) unalloyed uranium and (b) a low-silicon alloy during irradiation (original magnification, ×250) (McDonell, 1973).

affect cavitation. McDonell (1973) has proposed that intragranular cavities are formed in α-U by a basic mechanism similar to that of vacancy-void formation in irradiated nonfissile metals and, as such, is very sensitive to the metallurgical state of the fuel and to small alloy additions. Specifically, cavitational swelling can be drastically reduced by minor additions of silicon and aluminum (as shown in Fig. 5).

In contrast to swelling in the α-phase, swelling in the higher temperature phases occurs entirely by growth of fission gas bubbles except, of course, the swelling that takes place throughout all phases due to solid and liquid fission products (Claudson *et al.*, 1959; Greenwood, 1961). Fission gas is virtually insoluble in metallic U. Although a certain concentration of gas may be held in dynamic solution as a result of fissioning, fission gas will precipitate as bubble nuclei, some of which then grow by acquiring more gas atoms and vacancies, while others are redissolved by neighboring fission events. At some burnup when sufficient fission gas has been generated, the larger nuclei become gas bubbles that tend to maintain an equilibrium gas pressure by balancing the internal gas pressure (P_i) against the bubble surface tension (γ) and the external pressure (P_{ex}) through

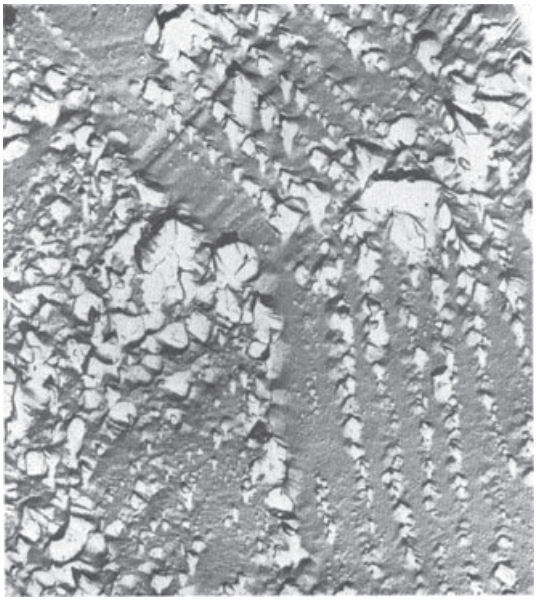

Fig. 6 Crystallographically aligned tears are uranium-irradiated at 575 °C to 0.1 at.% burnup (Leggett, 1967).

growth – an increase in bubble radius (r) – according to the following equilibrium relation:

$$P_i = P_{ex} + \frac{2\gamma}{r} \quad (1)$$

The external pressure is determined by the plastic flow characteristics of the fuel surrounding the bubble (Enderby, 1956), the pressure of the medium external to the fuel (Kulcinsky *et al.*, 1969; Lehmann *et al.*, 1969; Leggett *et al.*, 1966), or the mechanical restraint of the cladding when in contact with the fuel. This mechanism can lead to very high swelling rates at high temperatures where fission gas diffusivity and vacancy mobility are high and the fuel matrix strength, which in externally unrestrained fuel determines P_{ex}, is low, as is the case for the γ-phase. Externally unrestrained swelling of the various allotropes of U at low burnup (i.e., below ∼1 at.%) varies with temperature, as shown in Fig. 7.

Excessive swelling in both the cavitation region and the high-temperature fission-gas bubble region is, of course, prevented in fuel elements by a suitable cladding. Since the primary function of cladding is to provide a radiological barrier between fuel and coolant, it should also be designed to withstand the stress resulting from its secondary role as a restraint to fuel swelling. It is clear from Eq. (1) that if more free volume is provided for swelling fuel within the confines of the cladding, the internal gas pressure (P_i) will be lower at a given burnup. At an appreciable average bubble size, γ/r will be relatively small, and the external pressure (P_{ex}), provided by cladding restraint, will then be nearly equal to P_i. This model was evaluated by Blake (1961), who showed that a burnup of ∼5 at.% (at that time this was a significant improvement) was achievable with metallic fuel if 30–40% free volume was provided for fuel swelling.

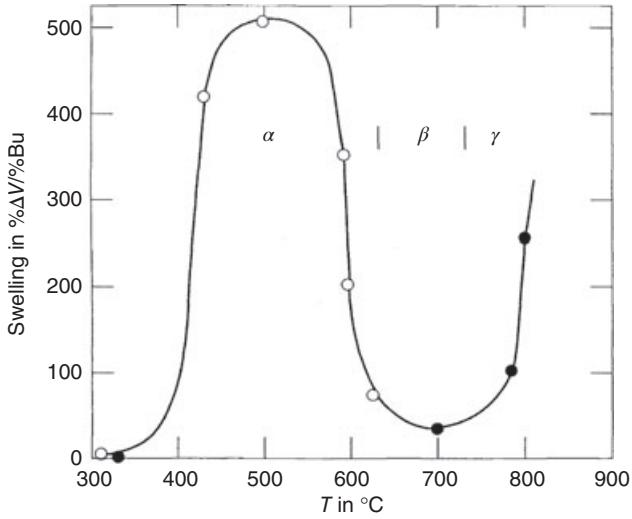

Fig. 7 Swelling rate of U phases in a burnup range of 0.2 to 0.5 at.%.

Blake did not consider gas release in his model, but when Beck (1968), following a suggestion by Barnes (1958, 1964), showed that most of the fission gas was released from the fuel at ~30% swelling, it was clear that the pressure inside the fuel element could be decreased by providing a plenum for this gas. Given a fuel element with a gas plenum volume equal to the original fuel volume (plenum-to-fuel volume ratio of 1), Blake's model results in the cladding pressure loading and strains, with and without gas release (see Fig. 8). Although the actual cladding stress and strain depend on the dimensions and type of cladding used, and also on irradiation-enhanced

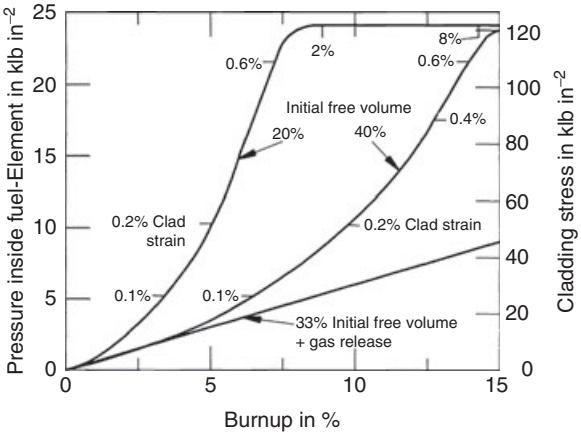

Fig. 8 Variation of fuel pressure inside cladding as a function of burnup (Blake, 1961). Nimonic at 500 °C, wall-diameter ratio: 0.09 (1 klb in^{-2} ≈ 6.9 × 10^6 Pa).

creep and swelling of the cladding (which Blake did not consider), it is clear that the large reduction in cladding deformation due to gas release makes truly high burnup operation possible.

2.2 Uranium–Plutonium

Plutonium is soluble in concentrations of up to 16% in α-U and, as shown in Fig. 3, the α-U phase retains its anisotropic characteristics. Plutonium is soluble up to 20% in β-U and completely soluble in γ-U. Alloys with up to 16% Pu can, therefore, be expected to have swellings behavior similar to that of U. Irradiation tests have confirmed this (Pugh, 1961): cavitation dominates in the α-phase, whereas rapid fission-gas bubble growth dominates in the γ-phase. It appears that adding Pu enhances the swelling rate in each of the phases, presumably because Pu increases the diffusivity of the alloy and decreases its creep strength. At higher Pu concentrations, the orthorhombic α-phase transforms to the tetragonal ζ-phase and, as a result, the cavitational component diminishes as the anisotropic α-phase disappears. Binary U–Pu alloys, however, are not suitable for high-temperature applications because of the eutectics that Pu forms with commonly used iron- and nickel-based cladding materials.

2.3 Thorium–Uranium (Plutonium)

As the only nonfissile major actinide element, thorium requires the addition of U or Pu (or both) to function as a fissile metal. U has limited solubility in Th (Fig. 9) and a Th–U alloy will consist of a dispersion of fissile particles in a fertile Th matrix, as shown for a 10 or 20% alloy in Fig. 10. Because of the small size of the U precipitates, nearly all fission fragments will recoil into the surrounding Th. Likewise, any fission from U-232 in the Th will result in recoil damage in the Th matrix. One would expect, therefore, that the swelling behavior of Th–U alloys to have the characteristics of a high-melting cubic material and to be isotropic.

The results of a later, high-temperature irradiation by Kittel and Horak (1961) are shown in Fig. 11. It appears that when the U alloy fraction becomes appreciable (>25%) the irradiation behavior of the U-phase renders the overall alloy behavior less stable. Because plutonium is highly soluble in Th, one expects an alloy of Th–U–Pu to exhibit an isotropic swelling behavior. The results of a single test with these alloys by Blumenthal *et al.* (1969) appeared to confirm this. The swelling behavior is similar to the cubic fuel alloy at high temperature, as shown in Table 1.

2.4 Alloys with Nonfissile and Nonfertile Constituents

A great deal of effort has gone into attempts to reduce the swelling of U by alloying. By and large, these studies have been successful in delaying the onset of high swelling rates to burnups that are high enough to yield

Tab. 1 Swelling of cast Th–U rods versus burnup and temperature (Kittel and Horak, 1961).

Rod number	*1*	*2*	*3*	*4*	*5*
U (wt%)	10	15	20	25	28
Burnup (at.%)	4.5	4.9	4.9	5.1	8.2
Temperature (°C)	700	700	700	700	>850
Swelling (%)	1.6	2.1	2.4	3.6	10.5

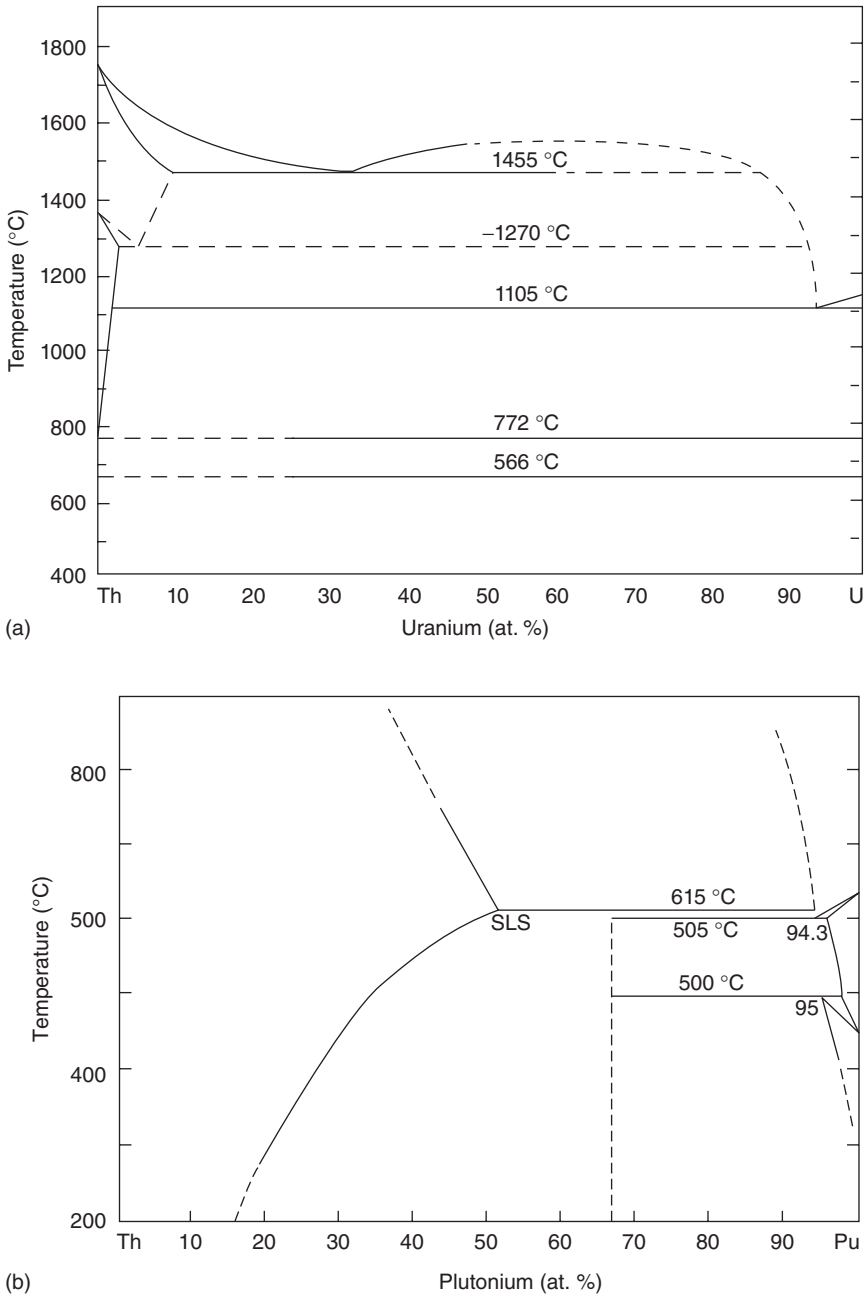

Fig. 9 (a) Th–U and (b) Th–Pu phase diagrams. After Rough and Bauer (1958).

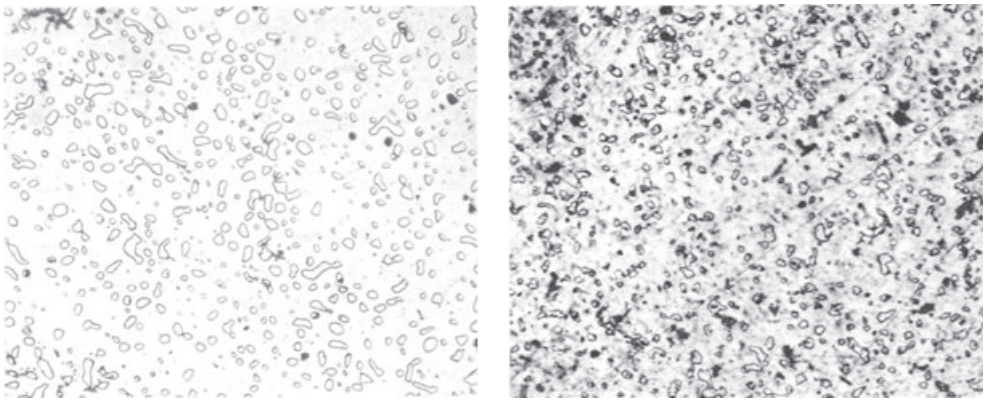

Fig. 10 Effect of irradiation on microstructure of Th–20U–10Pu alloy. (a) Unirradiated. (b) At 5.68 at.% burnup. After Blumenthal *et al.* (1969).

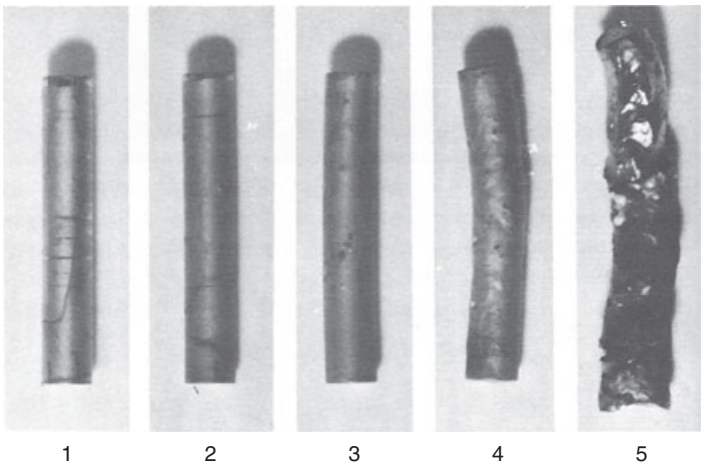

Fig. 11 Effect of high-temperature irradiation on cast Th–U alloys. The numbers identify the alloy specimens listed in Table 3. After Kittel and Horak (1961).

satisfactory fuel performance in thermal reactors. This has led to the development of an "adjusted" U – that is, U alloyed with small amounts of Al, Fe, or Si (Jepson and Slattery, 1961; Barnes, 1964; McDonell and Angerman, 1965; McDonell, 1965, 1973; Lehmann *et al.*, 1969). These minor elements form small precipitate phases that appear to control point defect behavior and grain size, thereby reducing the low-burnup tearing phenomenon (see Fig. 3). However, similar attempts to achieve the capability for high burnup (i.e., above a few at.%) for fast reactor fuels have not been successful in reducing swelling to levels low enough to prevent fuel-cladding contact. The buildup of fission-gas pressure in the fuel during continued irradiation

after fuel-cladding contact eventually results in an unacceptable stress in the cladding.

However, as mentioned earlier, high burnup in fast reactor fuels can be achieved by allowing enough room for swelling within the cladding to release the pent-up gas to a plenum. It therefore appears unnecessary to employ alloy additions solely to control the swelling of metallic fuel for fast reactors. While the swelling rate *per se* is not important to ensure high-burnup capability, knowledge of the effect of these alloy additions on swelling is required in order to predict swelling behavior and fission gas release, to model fuel element behavior, and to perform reactor physics calculations. Of course, fuel is alloyed for other reasons. For example, it has been necessary to add Zr to U and U–Pu fuels to improve their chemical compatibility with steel cladding, while the pyrometallurgical refining of spent fuel effectively results in an alloy of certain fission products and the fuel, as the irradiated fuel is recycled.

Studies on higher U alloys has centered on elements that form extensive solid solutions with U in the high-temperature γ-phase, specifically Mo, Zr, Ti, and Nb. These elements lower the temperature of the cubic γ-phase boundary, allowing more of the fuel to operate in the isotropic γ-phase; they also increase the solidus temperature, raising the margins at which the fuel melts.

The swelling behavior of these alloys at low burnup is associated with the relative stability of the γ-phase, as illustrated in Fig. 12 (Thomas *et al.*, 1958). The γ-phase of U–Nb decomposes very quickly into two phases dominated by the isotropic α-phase, even at moderate temperatures, and the swelling is characterized by rapid cavitation in the α-phase, similar to that of α-U in the 300–400 °C range. As the swelling curves (Fig. 13) show, the addition of Zr stabilizes the γ-phase and appears to suppress the excessive swelling in the cavitation stage of this alloy.

Although U–Mo is more stable than U–Nb, its swelling behavior (Fig. 13) is largely due to the effect of irradiation on the α ↔ γ-phase transformation. It has been shown by Kittel *et al.* (1964), Bleiberg, Jones, and Lustman (1959), and Kryger (1969) that, at sufficiently high fission rates, the γ-phase is stable to very low temperatures. Cavitation under such conditions is completely suppressed, and high swelling rates in this alloy occur at high temperature as a result of gas bubble formation in the γ-phase. As is the case for pure uranium, cavitation swelling in alloys may also be reduced

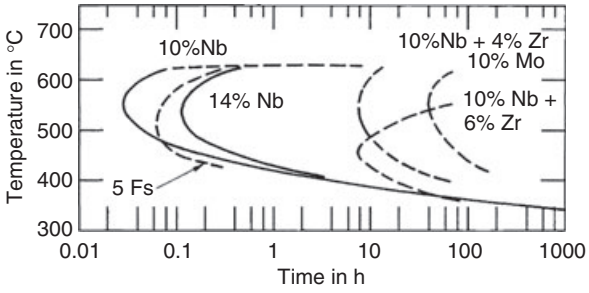

Fig. 12 Start of transformation of γ-uranium alloys, solution heat-treated at 900 °C (Thomas *et al.*, 1958).

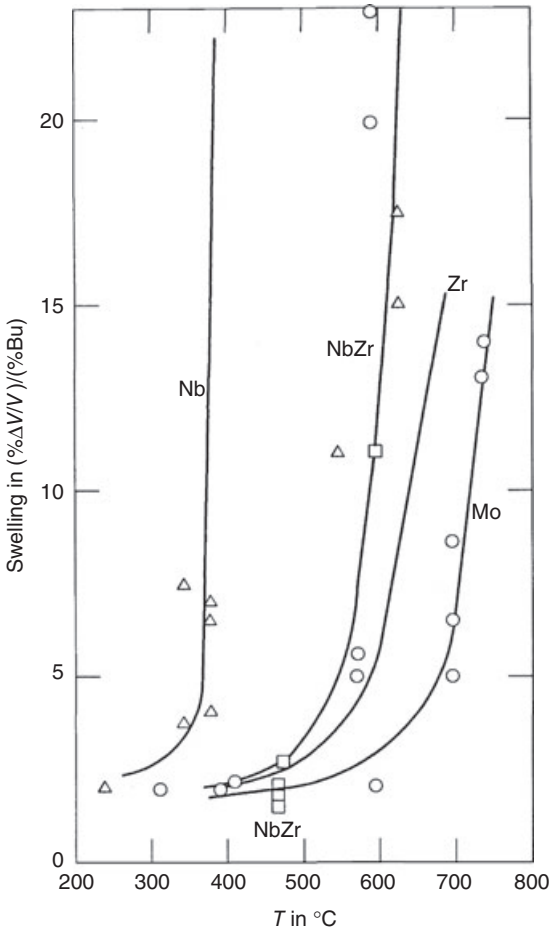

Fig. 13 Swelling rate of various γ-stabilized uranium alloys as a function of the irradiation temperature.

through the addition of minor third elements such as Si, Al, and Fe. This has been achieved, for example, in U–Fs (basically a U–Ru–Mo alloy), resulting in a change in swelling behavior, as shown in Fig. 14.

Attempts to reduce the swelling of Pu-containing fuels for fast breeder reactors by means of alloying have been generally unsuccessful. Researchers in the United Kingdom (Frost *et al.*, 1962) and France (Mustelier, 1962) concentrated on U–Pu–Mo, basing their choice on prior experience with U–Mo alloys. Large swelling, as much as 100%, occurred in these alloys at burnups of ~1 at.% in the temperature range of interest, 500–700 °C. The swelling was due to extensive fission gas porosity similar to that found in high-temperature γ-U irradiations. Studies conducted in the United States focused on U–Pu–Fs, U–Pu–Ti, and U–Pu–Zr, with similar results (Horak *et al.*, 1962; Beck, 1968).

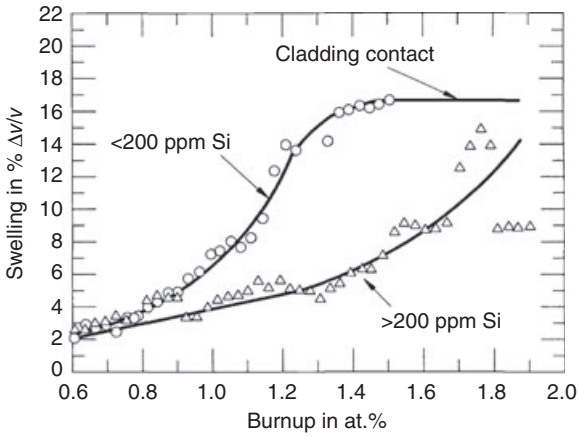

Fig. 14 Effects of Si on fuel swelling of U–5 wt% Fs as a function of burnup.

Although, to repeat once more, there is no longer a need to reduce swelling to achieve a high burnup, these experiments were important in characterizing the development of interconnected porosity and attendant gas release in various alloys. The correlation of gas release with swelling appears to be rather independent of fuel alloy, as shown in Fig. 15. In addition, the swelling rates obtained from these experiments were useful in determining fuel length increases and burnup to fuel-cladding contact for subsequent fuel element designs.

A renewed interest in high-density fuel for the conversion of test reactors from HEU to LEU has expanded the understanding of the low-temperature behavior of U-alloys, in particular U–6–10% Mo. These fuels are developed as dispersions (see Chapter Fission Gas and Bias-Driven Swelling of Nuclear Fuels) and as solid laminated plates and rod types operating at very high fission rates and temperatures below 300° C (Lemoine *et al.*, 2007). Fuel swelling data now extend to 20 at.% U burnup or about 7×10^{27} fission m^{-3}, as shown in Fig. 16.

Several interesting discoveries were made during the course of this fuel development effort. As shown in the micrographs in Fig. 16, at the lower burnup the behavior of fission gas is characterized by the formation of bubbles at the alloy grain boundaries. These bubbles account for only a small percentage of the fission gas generated. Subsequent transmission electron microscopy (TEM) examination revealed the form of the majority of the fission gas in the alloy grains; as shown in Fig. 17 (Gan *et al.*, 2010), the fission gas existed as ~2-μm precipitates arranged in a regular three-dimensional lattice.

Such "bubble lattices" have never been observed in irradiated fuel, but they are well documented in ion-irradiated metals (Johnson *et al.*, 1997). At higher burnup, the alloys were found to exhibit grain refinement similar to what has been seen in UO_2 (see Chapter Fission Gas and Bias-Driven Swelling of Nuclear Fuels).

2.5 Alloys Containing Minor Actinides

The recycling or "burning" of the minor actinides (Np, Am, and Cm) that are

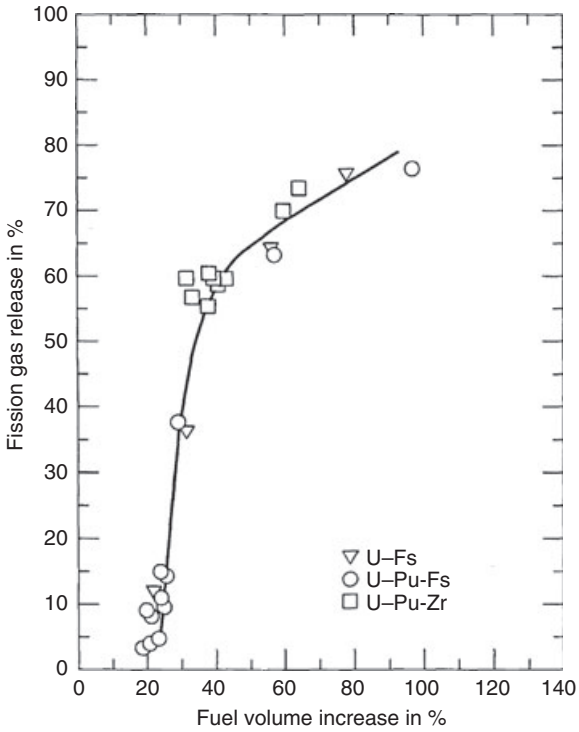

Fig. 15 Fission-gas release versus fuel-volume increase. After Beck (1968).

extracted with Pu and U from spent fuel has recently received renewed attention. Several irradiations are in progress in the Advanced Test Reactor in Idaho, and one irradiation has been completed in the Phenix reactor in France. However, no detailed post-irradiation data are yet available.

Towards the final stage of the IFR fuel development, a series of U–Pu–Zr alloys containing small amounts of Np and Am were designed. Unfortunately, post-irradiation data of only the first of these test fuel elements are currently available.

As shown in Fig. 18, the cross-section of the irradiated fuel is comprised of the familiar three-zone microstructure with the radial redistribution of Zr and U. The behavior of Np and Am appears to be very different. Np, being rather soluble in U and Pu, is behaving very much like Pu, whereas Am with a very low solubility in the actinide alloy appears to collect in pores in both the central and peripheral zones.

2.6 U–Pu–Zr Alloy Fuels for Fast Reactors

Metallic fuels were the first to be used in fast reactors, an example being the EBR and its successor EBR-II in the United States (Monson, 1967), and in the DFR in the United Kingdom (Henry and Edwards, 1966). During the mid-1960s, worldwide interest turned to oxide fuels because of their greater burnup capability before the full potential of metallic fuel could be achieved. However, development continued

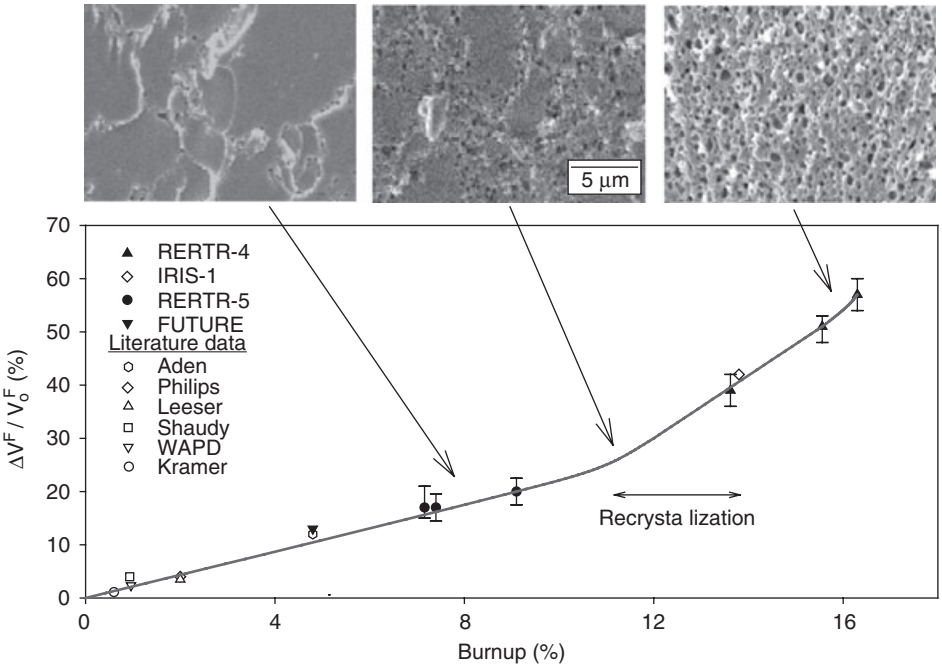

Fig. 16 Swelling and fission gas bubbles in U–Mo as a function of burnup.

at EBR-II because this reactor continued to be fueled with a metallic U-fissium alloy, U–5 Fs.[4)] During the 1970s, the burnup limitations of this fuel were satisfactorily resolved and additional attributes of metallic fuel were discovered, as reviewed by Walters *et al.* (1984).

In 1983, a concept termed the integral fast reactor emerged at ANL (Till and Chang, 1988) which offered a safe and economic reactor with significant safety benefits that derived from the high thermal conductivity of its metal fuel (Cahalan *et al.*, 1985; Marchaterre *et al.*, 1985, 1986; Wade and Chang, 1988). The U–Pu–Zr system, which had been tested in the late 1960s, was the obvious fuel choice. The safety benefits of the IFR were demonstrated by two tests at EBR-II; in one test a loss of primary flow at full power without scram was simulated, while in the other test a loss of heat sink without scram was simulated. In both cases the reactor shut itself down without operator or mechanical intervention (Mohr *et al.*, 1987; Planchon *et al.*, 1987).

The key step in reprocessing IFR metallic fuel is electrorefining (Burris, 1986; Burris *et al.*, 1984, 1986). The cathode product contains U, Pu and the minor actinides, along with enough residual fission products to keep the cathode product highly radioactive. Because these retained fission products keep the fuel highly radioactive, all reprocessing and re-fabrication steps are carried out remotely. Such reprocessing brings several benefits:

[4)] Fissium is an equilibrium concentration of fission products left by the pyrometallurgical reprocessing cycle used at EBR-II, and consists of 2.5 wt% molybdenum, 1.9 wt% ruthenium, 0.3 wt% rhodium, 0.2 wt% palladium, 0.1 wt% zirconium, and 0.01 wt% niobium.

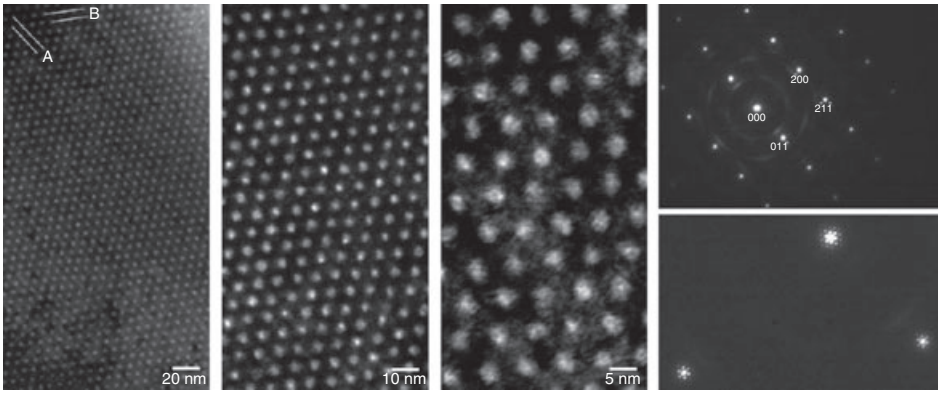

Fig. 17 Transmission electron microscopy images of a superlattice of fission gas bubbles in irradiated U–7Mo particle of bcc structure oriented at zone [011]. The selected-area diffraction (SAD) patterns show rings due to oxides formed at the U–7Mo fuel particle during sample preparation. An enlarged view of the SAD pattern (at right) shows satellite spots due to the bubble superlattice. After Gan *et al.* (2010).

- Diversion of the fuel is impossible as the material is highly radioactive; likewise, the process makes proliferation nonfeasible because the cathode product remains alloyed as well as radioactive.
- The process involves batch operations and is easily scaled to meet local or increasing reactor requirements.
- Perhaps most importantly, reprocessing allows essentially all actinides to remain in the fuel cycle, to be fabricated into new fuel elements and fissioned for useful energy (Chang, 1989). Without the actinides, the high-level waste from reprocessing will decay to background levels in only a few hundreds of years.

As the metallic alloy most recently under active study, U–Pu–Zr provides the most extensive set of data, although substantially older data for U–Fs and limited information on other alloys are available. The general swelling behavior for these alloys is shown in the increase of fuel pin length versus burnup in Fig. 19. Swelling proceeds rather rapidly with burnup, which is characteristic for metal fuel; U–Fs exhibits a somewhat lower rate because of the previously mentioned retarding effect of Si additions on swelling. Virtually all length increase takes place in the burnup interval before the swelling fuel contacts the cladding. The leveling-off in axial swelling is thus determined by the fuel smear density. The planar smear density is typically chosen at approximately 75% to allow sufficient swelling (~30%) to facilitate fission release gas from the fuel (Fig. 20). This level of planar swelling would, for isotropic swelling, translate to a length increase of ~16%, yet the observed length increases are consistently smaller, indicating anisotropic swelling. The main reason for this effect appears to be the difference in swelling behavior between the hotter center of the fuel pin and the colder periphery, as illustrated in Fig. 21 for U–10Zr (Hofman *et al.*, 1990).

In the center part of the fuel pin, where the γ-phase predominates, large gas bubbles form; this is indicative of a higher plasticity of the fuel and, therefore, a lower capability to sustain shear stresses. In

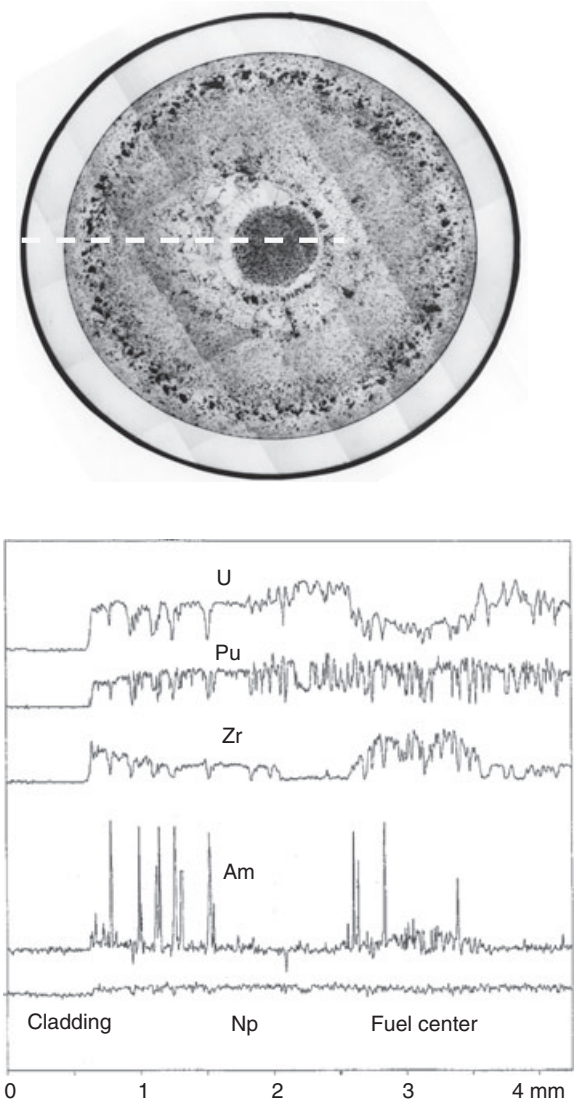

Fig. 18 Redistribution of actinides along the indicated scan in U20.2–Pu9.1–Zr1.2–Am1.3Np irradiated to ~6 at.% burnup.

the extreme case (if the center were to behave in a viscous manner), the fission gas pressure in the center would result in a near-biaxial loading of the peripheral shell, the radial stress component being twice the axial component. A stress effect on swelling in the peripheral fuel zone (predominantly α-phase) would result in a larger diametral than axial strain, and hence anisotropic swelling (Kobayashi *et al.*, 1990). Anisotropy is especially pronounced and variable in U–Pu–Zr, as

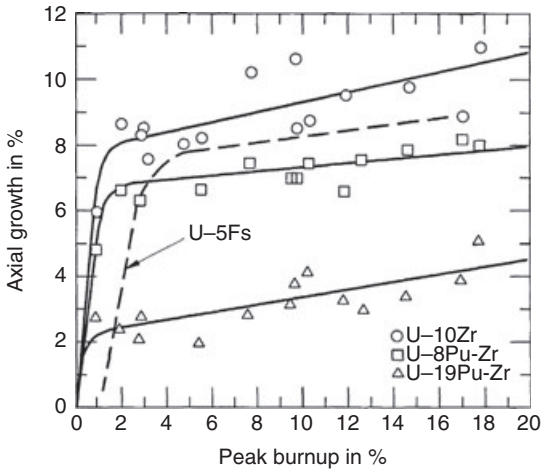

Fig. 19 Fuel length increases in various metallic fuels as a function of burnup (EBR-II irradiation).

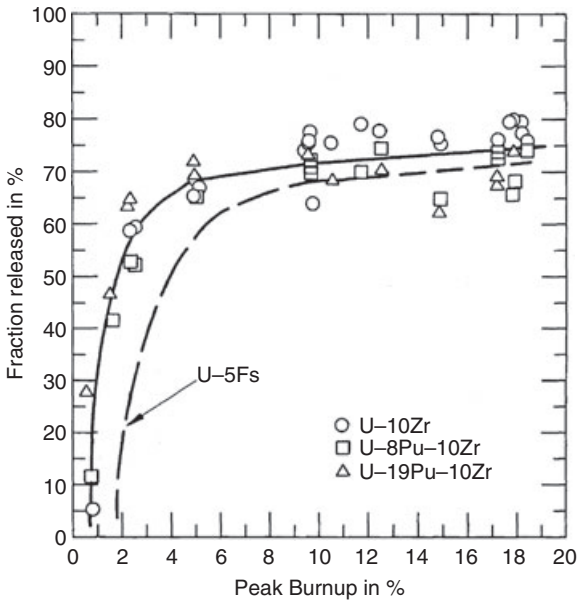

Fig. 20 Fission gas released to plenum above fuel for various metallic fuels as a function of burnup (EBR-II irradiation).

shown by the variation in axial fuel growth in Fig. 20.

The larger anisotropy (proportionally low axial swelling) in some of the higher Pu elements is due to a change in the various alloy phases present in radial zones. This change is a result of rather rapid Zr redistribution in the radial temperature gradient. The equilibrium phase diagram of U–Pu–Zr (see Fig. 22) shows that various

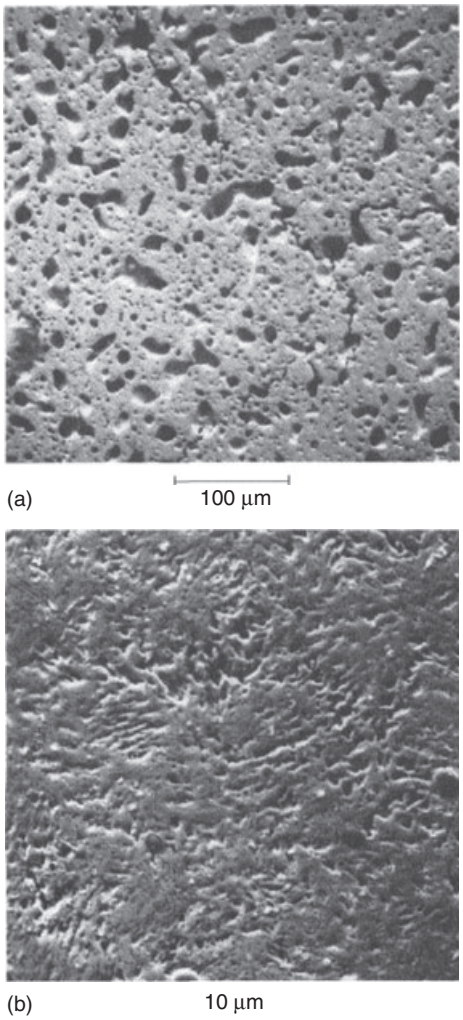

Fig. 21 Scanning electron microscopy images showing different pore morphologies in irradiated U–10Zr. (a) Predominantly γ-phase. (b) Predominantly α-phase.

phase field boundaries can be found radially across an operating fuel element. The solubility of Zr in these phases varies with temperature; thus, a driving force for diffusion can be created both by the gradient in chemical potential of the fuel constituents in these phases, and by the heat flow. A low Zr zone consisting primarily of the Pu ζ-phase is observed to form at the center of elements by Zr migration to the lower temperature Zr δ-phase at the periphery. In parts of fuel elements that operate at higher temperatures, this Zr-depleted zone forms at mid-radius by migration of Zr to both the high-temperature Zr γ-phase at the center and the Zr δ-phase at the periphery.

The location of the radial zones essentially follows isotherms in the fuel which are determined by the various phase boundaries of the alloy. In the usual situation of upward coolant flow and a cosine-shaped axial power profile in the fuel, the peak fuel temperature occurs between the center and top of the fuel column. An example of the resulting zone pattern in a moderate power U–19Pu–10Zr fuel element is shown in Fig. 23. In higher-power elements, the peak fuel temperature shifts to a higher axial position, while the three-zone pattern, with a Zr-depleted zone at an intermediate radial location, may be extended to the very top of the fuel column.

Alloy constituent migration in a temperature gradient – the so-called Soret effect – is rather difficult to measure experimentally in most alloy systems because of its extremely slow kinetics. However, such migration is commonly observed in power reactor fuel, owing to a combination of high-temperature gradients and, possibly, fission-enhanced diffusivity. Examples are fission product migration in mixed oxide fuel (Hehenkamp, 1977) and hydrogen redistribution in U–Zr hydride fuel (Merten *et al.*, 1963). The chemical driving force for the redistribution of a particular solute in a homogeneous solution held in a temperature gradient arises from the temperature dependence of the solute's chemical potential, and from energy transfer by conduction electrons and phonons. Such a system will tend to minimize its total

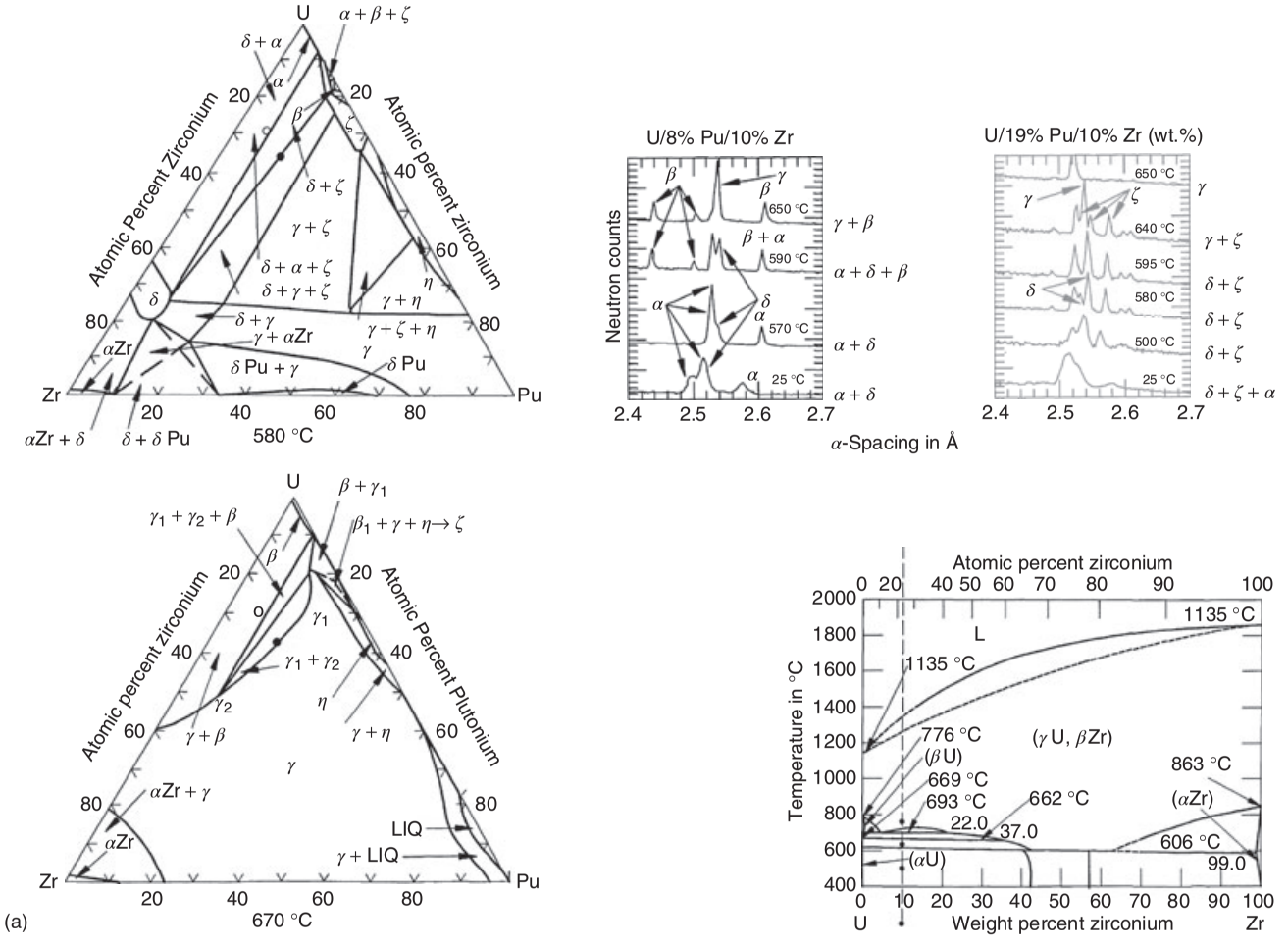

Fig. 22 Equilibrium phase diagrams of U–Zr, U–Pu–Zr, and selected neutron diffraction data for cast alloys (O'Boyle and Dwight, 1970).

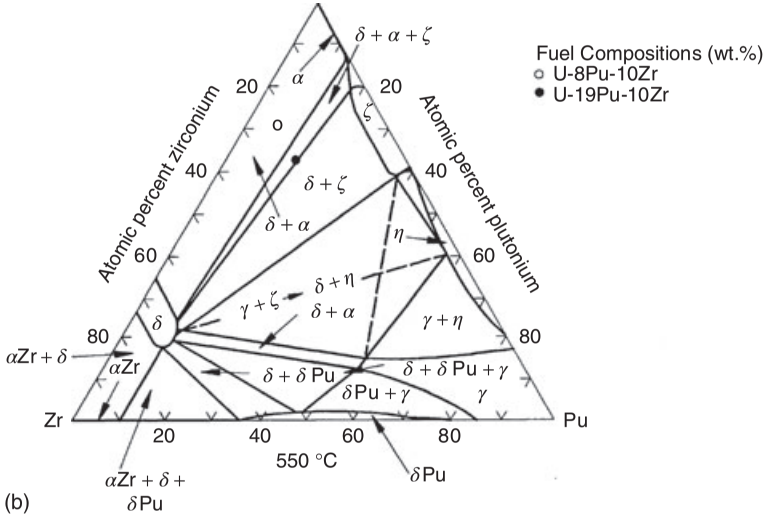

Fig. 22 (*Continued*).

Phase composition in mol% vs. temperature for U-10%Zr fuel pin

T in °C	α	δ	β	γ
25	88 %	11 %	-	-
500	72	26	-	-
635	71	-	-	27 %
750	-	-	-	99

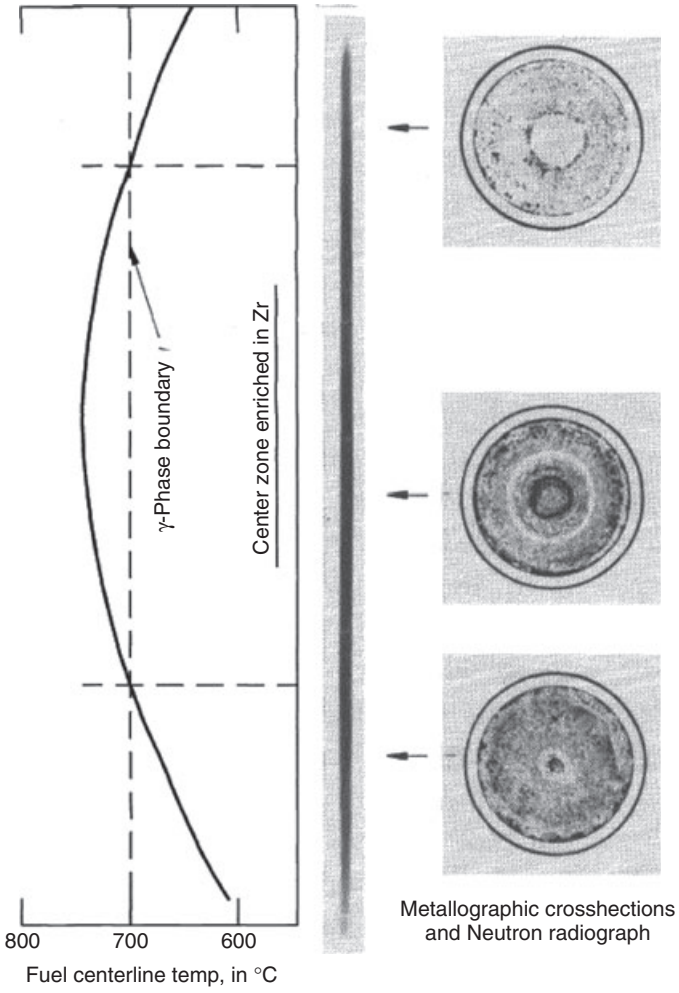

Fig. 23 Axial temperature profile along the centerline of U–19Pu–10Zr element at 17 at.% burnup, and its relation to the radial zone patterns shown in a neutron radiograph and three cross-sections.

free energy by adjusting its composition, thereby producing a chemical potential that is constant. The solute flux in a temperature gradient is characterized by a phenomenological parameter, called the heat of transport, Q^*, of the migrating solute according to Fick's first law:

$$J_i = \frac{-D_i N_i}{RT}\left(\frac{RT\partial \ln N_i}{\partial x} + \frac{Q^*}{T}\frac{\mathrm{d}T}{\mathrm{d}x}\right) \quad (2)$$

where D_i and N_i are the diffusivity and concentration of the migrating solute, respectively.

According to current theory, the heat of transport consists of three components, where $Q^* = Q_{\mathrm{in}} + Q_{\mathrm{e}} + Q_{\mathrm{p}}$, with Q_{in} being an intrinsic component and Q_{e} and Q_{p} being attributed to the electron "wind" and phonon "wind," respectively (Wever, 1973).

The heat of transport can be either positive or negative, depending on the sign and magnitude of its components. For example, the value of Q^* for pure U was measured to be $+5\,\text{kcal mol}^{-1}$ (ca. $+21\,\text{kJ mol}^{-1}$) (D'Amico and Huntington, 1969), and to be $-34\,\text{kcal mol}^{-1}$ (ca. $-143\,\text{kJ mol}^{-1}$) for Zr (Campbell and Huntington, 1969). In their pure states, U moves down a temperature gradient while Zr moves up, but whether this has any significance for a U–Zr alloy could not be speculated. Thus far, a valid model that takes into account all contributions to Q^* has eluded researchers. In the absence of such a model that is capable of predicting the direction and magnitude of thermomigration in present-day fuel alloys, a phenomenological approach developed by Shewmon (1958) for two-phase alloys may be used to explain these observations. With the appropriate assumptions, Eq. (2) may be written as

$$J_i = -\frac{DN_i}{RT^2}(\Delta H_i + Q^*)\frac{\mathrm{d}T}{\mathrm{d}x} \tag{3}$$

where ΔH_i is the partial molar enthalpy of solution for component i. The migration direction is thus determined by the sign of the sum $(\Delta H_i + Q_i^*)$.

According to this theory (considering Zr only), $(\Delta H_{zr} + Q_{zr}^*) < 0$ in the high-temperature γ-phase fields and $(\Delta H_{zr} + Q_{zr}^*) > 0$ in the $(\beta + \gamma)$-phase field, leading to the observed Zr enrichment at the center of the fuel and a depletion of Zr in the intermediate (original $\beta + \gamma$) zone, as shown in Fig. 24. At lower fuel centerline temperatures, when the γ-phase is absent, only outward Zr migration occurs, resulting in a Zr-depleted center (the original $\beta + \gamma$) zone.

The rate of Zr redistribution in low-Pu fuel (i.e., 3% and 8%) is essentially similar to the rate in U–10Zr, but it is much more

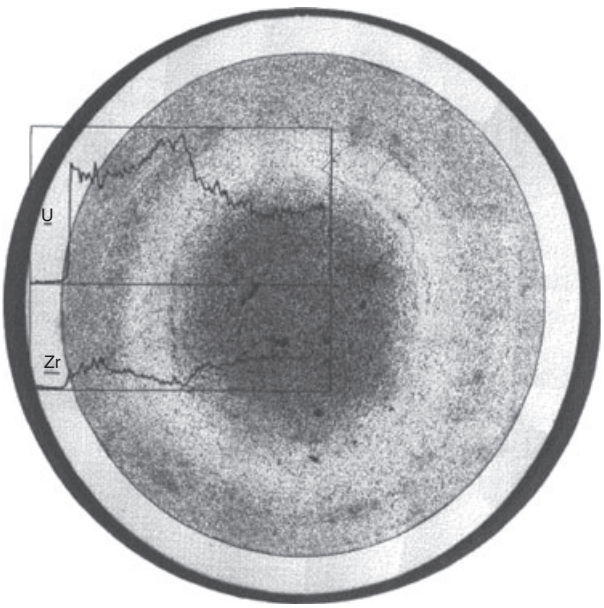

Fig. 24 Transverse metallographic section from the high-temperature region of an U–10Zr element at 5 at.% burnup, with superimposed microprobe scans showing zone formation and Zr–U redistribution.

rapid for Pu concentrations of 19% and higher. This is illustrated in Fig. 25 for a fuel element at ~3 at.% burnup that was irradiated at a power density (i.e., temperature gradient and fission rate) similar to that applied to the binary U–10Zr element shown in Fig. 25. Either a higher Zr diffusivity in these higher-Pu alloys, or a larger thermodynamic force due to the presence of the Pu ζ-phase, may account for this more rapid redistribution. The effect of the magnitude of the temperature gradient, dT/dx, and the effect of fission rate on the diffusivity, D (two parameters that cannot be separated in the present tests), on the kinetics of the redistribution phenomenon is evident from the observation that significant Zr migration and zone formation in *lower* power density high-Pu fuel elements is delayed to higher (~5–6 at.%) burnup (Porter *et al.*, 1990).

If, as in high-Pu high-power density fuel elements, zone formation occurs rapidly (i.e., early on in the irradiation during the swelling stage prior to fuel-cladding contact), this markedly enhances the rate of radial swelling. This high rate of radial swelling creates stresses in the peripheral fuel that are large enough to result in crack formation (as shown in Fig. 26) and also to increase the swelling anisotropy.

The porosity development in metallic liquid-metal-cooled fast reactor (LMR) fuel depends on the phases present in the fuel. In all alloys, the high-temperature cubic U γ-phase exhibits the characteristic large interconnected bubbles similar to those observed in pure γ uranium, whereas at lower temperatures, where the U α-phase predominates, the characteristic tearing-type porosity is evident. In the U–Zr and U–Pu–Zr alloys, the

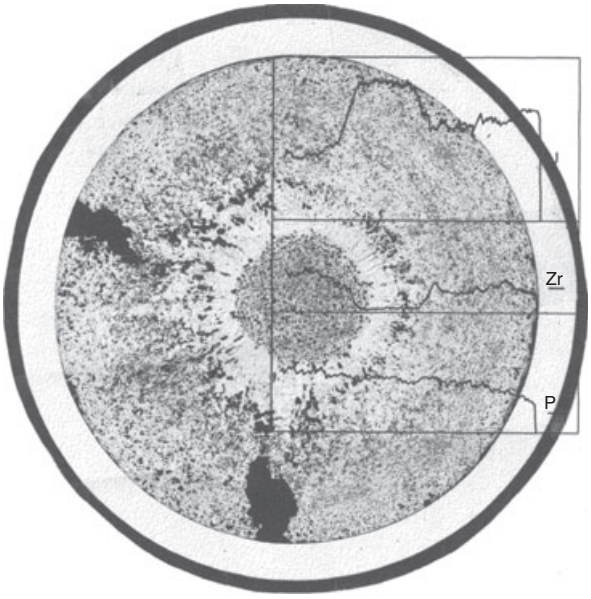

Fig. 25 Transverse metallographic section from the high-temperature region of an U–19Pu–10Zr element at 3 at.% burnup with superimposed microprobe scans, showing zone formation, cracking, and Zr–U redistribution.

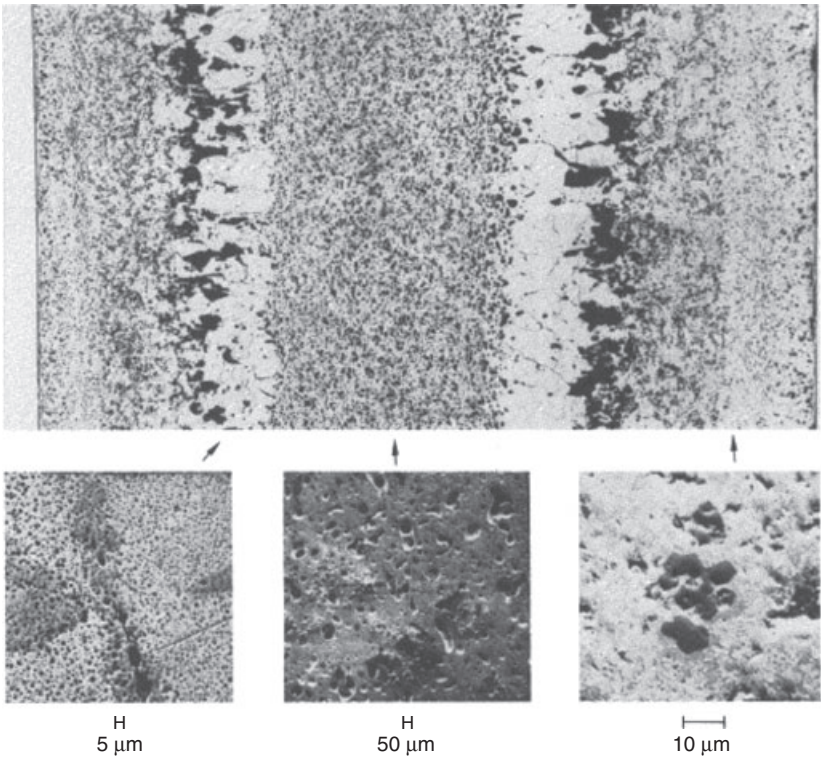

Fig. 26 Redistribution and zone formation in U–19Pu–10Zr fuel at 3 at.% burnup. The upper image shows the axial optical metallographic section; the lower images show scanning electron microscopy details of the zone microstructures (Hofman, 1980).

low-temperature U α-phase and Zr δ-phase form a laminar microstructure with rather smaller interlaminar spacing in U–Zr than in U–Pu–Zr, and the pore morphology follows this microstructure. In U–Fs, the microstructure is more equiaxed and the pore morphology appears to be more random. Examples of both high- and low-temperature porosity in U–Zr and U–Pu–Zr fuels are shown in Figs 21 and 26. When Zr redistribution and phasal zone formation occurs, the resultant low Zr–Pu β-phase and Pu ζ-phase have their own very fine pore morphology, an apparent characteristic of many intermetallic compounds (Hofman *et al.*, 1986).

A correct description or model of swelling and gas release should include the behavior of the various phases present, and thus requires a rather precise thermal calculation to determine the phase fields in the fuel element. A model for the redistribution of alloy constituents and determination of the formation of new phases such as the ζ-phase in U–PU–Zr is also essential. These needs call attention to the difficulty of determining the thermal conductivity of the fuel during irradiation, which is a classic problem in the modeling of any fuel element. For example, the thermal conductivity of mixed oxide fast reactor fuel changes during irradiation due

to porosity formation, fuel restructuring, stoichiometry changes, buildup of fission products, and changing fuel-cladding gap conductance. The satisfactory description of these changes in mixed-oxide fuel has involved a great deal of effort, and the evaluation of thermal conductivity of metallic fuel is fraught with similar difficulties. With porosity in the various microstructural zones of the fuel element now well characterized by post-irradiation examination, the drop in thermal conductivity due to porosity can be calculated with existing models (Di Novi, 1972). The gap conductance in sodium-bonded metallic fuel elements is very high and plays no significant role in the overall thermal calculation. If, however, the sodium bond were to be locally displaced by fission gas then the gap conductance would decrease at these locations. This type of displacement appears plausible, as evidenced by local irregularities in the fuel microstructures commonly observed in post-irradiation metallography of *high*-Pu elements that exhibit the aforementioned rapid redistribution and cracking; however, such irregularities are not observed in fuel elements not afflicted by the cracking phenomenon. For example, U–10Zr fuel axially develops a cone-shaped zone structure that follows isotherms within the fuel.

The bond sodium plays another important role in the course of the thermal behavior of the fuel during irradiation. When the fuel swells, it displaces the bond sodium from the gap to the gas plenum above the fuel. This in itself should have no effect on the fuel temperature, but near the point where the fuel reaches its maximum swelling the porosity in most of the fuel interconnects and gas is vented to the plenum. This allows the bond sodium to infiltrate the fuel body and increase the fuel's overall thermal conductivity. Such sodium infiltration is routinely observed in post-irradiation examination. The sodium level above the fuel elements, where the fuel has swelled out to the cladding, is always substantially lower than the total amount of preloaded sodium would indicate. Chemical analysis of irradiated fuel finds this "missing" sodium distributed throughout the fuel pin. On average, approximately 15–20% of the porosity is "logged" (filled) with sodium, resulting in the following course during irradiation. The overall thermal conductivity of the fuel drops continuously during the early free-swelling stage, due to porosity development, but then increases rather suddenly with gas release and sodium logging. This has been demonstrated by measuring the radial temperature drop in U–5Fs elements that were equipped with thermocouples at the fuel center and outer cladding surface, both in EBR-II (Betten, 1985) and in the ANL Chicago pile no. 5 reactor (CP-5) reactor (see Fig. 27) (Beck and Foussek, 1969). An analysis of these and other data (Betten, 1985) has led to a correlation of relative fuel thermal conductivity for use in fuel element modeling.

Further changes at high burnup depend primarily on the type of cladding used. High-swelling cladding such as austenitic stainless steel allows the fuel further radial swelling, which in turn provides additional room for solid fission product buildup. In contrast, with low-swelling cladding, such as martensitic HT-9 steel, the porosity gradually decreases due to the buildup of these fission products.

Another aberration in the thermal conductivity of the fuel sometimes occurs at transverse cracks that might form at various locations along the fuel pin. An example of this is shown in Fig. 28. From the variation

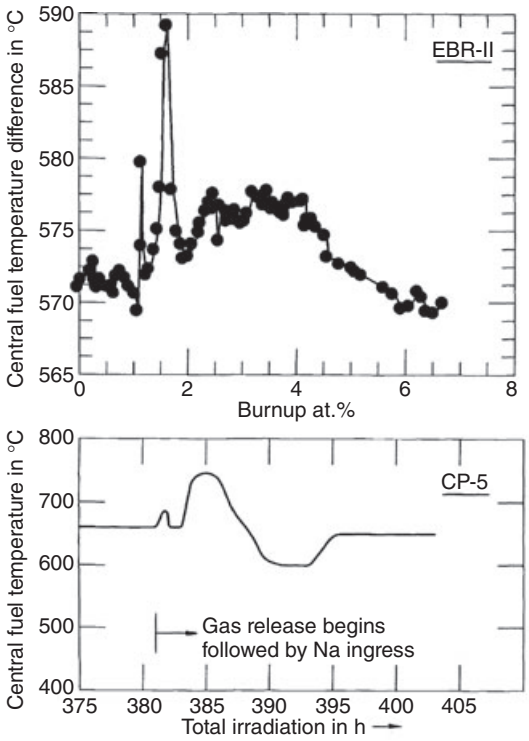

Fig. 27 Central fuel temperatures measured in instrumented U–5Fs fuel elements in (a) EBR-II (Betten, 1985) and (b) CP-5 (Beck and Foussek, 1969), showing the effects of gas release and sodium ingress into the swollen fuel on thermal conductivity.

in radial microstructural zone location, it appears that less sodium was logged at the crack, probably because of locally trapped fission gas.

3
Fuel–Cladding Interaction

3.1
Fuel–Cladding Mechanical Interaction

Fuel–cladding interaction that may result in cladding failure can be both mechanical and chemical. Fuel–cladding mechanical interaction (FCMI) arises from applied stress when the element design is an attempt to restrain fuel swelling, and may result in plastic deformation of the cladding.

As discussed in Section 2.1, the major source of stress in metallic fuel elements is the buildup of fission gas in bubbles and/or existing tears. The internal fission gas pressure builds up rapidly with burnup, and metallic fuel is rather plastic during fissioning. Because early element designs did not allow the fuel sufficient free swelling, this gas bubble pressure was transmitted directly to the cladding, and consequently all early designs suffered from cladding deformation and rupture at modest burnups. However, as discussed earlier and illustrated in Fig. 15, an as-built

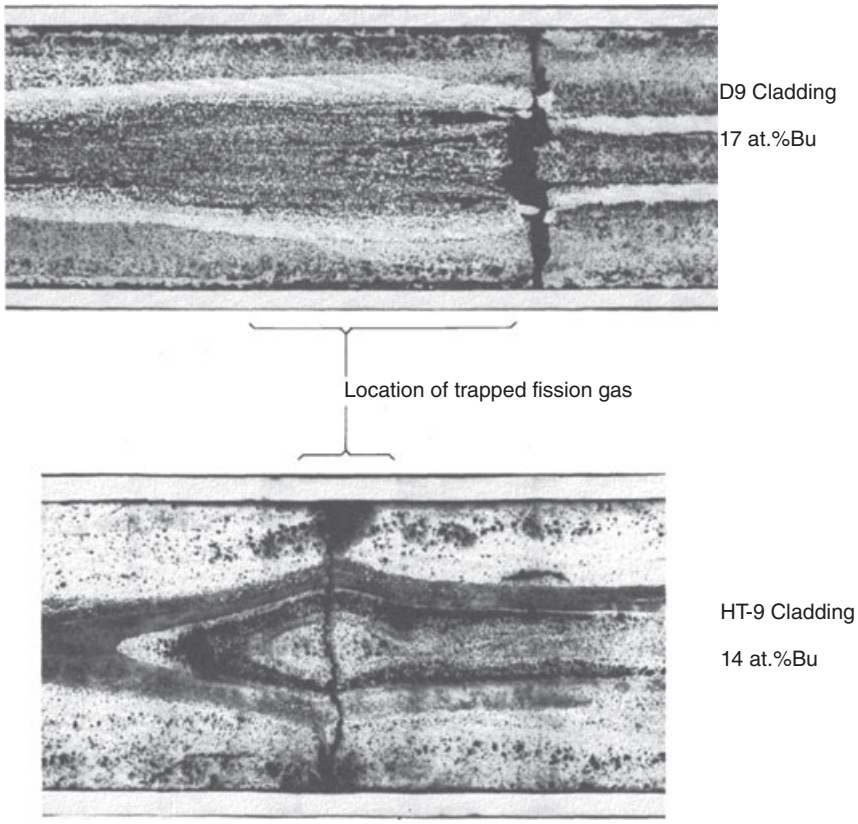

Fig. 28 Longitudinal section of U–19Pu–10Zr elements at high burnup, showing variations in radial zone location due to local differential heat transfer. The lower image shows the etched sample; the upper image shows the sample as-polished.

smeared density of about 75% allows free fuel swelling of approximately 30%, at which point porosity becomes largely interconnected and open to the outside of the fuel, releasing a large fraction of the fission gas to a suitably large plenum at the top of the element. The gas pressure in the open pores is then determined by the volume and temperature of the plenum above the fuel. A series of irradiation experiments was performed in the CP-5 reactor to test this idea (Beck, 1968). Elements containing U–Pu–Fs, U–Pu–Ti and U–Pu–Zr were included in this test, with a variety of cladding materials and a range of smeared densities and plenum volumes. If the effects of fuel–cladding chemical interaction (FCCI), specifically for the U–Pu–Fs fuel (to be discussed later) are excluded, a consistent picture emerges from these tests. A high burnup operation (in excess of 10 at.% without cladding failure) is achievable with smeared densities of 75% or lower and a plenum-to-fuel volume ratio of 0.6 or higher. A subsequent test based on these parameters with U–Pu–Zr elements was successfully run in EBR-II (Murphy *et al.*, 1969). Based on these confirmatory results, the EBR-II driver fuel element design was changed from the MK-IA to the MK-II

type, employing smeared densities of 86% and 75% and plenum-to-fuel volume ratios of 0.15 and 0.8, respectively. The difference in cladding deformation of the two element designs, both of which consisted of U–5Fs fuel and type 304 stainless steel cladding, is shown in Fig. 29.

The cladding strain of the low-smear density, small-plenum MK-IA design is primarily creep strain due to FCMI, while that of the MK-II elements is mainly irradiation-induced cladding swelling. The creep strain in the MK-II elements can be accounted for by the plenum pressure stress alone, which confirms that FCMI is virtually nonexistent in suitably designed metallic fuel elements, and that cladding stress is determined by the fission gas pressure in the interconnected porosity.

Since the presence of open (interconnected) fission gas porosity appears to be a key feature in reducing FCMI, the question arises as to what the effect of accumulation of low-density solid fission products on this porosity might be at high burnup. The following discussion shows an approximate calculation of the net volume change due to nongaseous fission product accumulation.

The total fission yield of the major fission products is shown in Table 2. A rigorous analysis of the change in molar volume of the fuel due to transmutation of uranium and plutonium into solid fission products requires an evaluation of their chemical state in the various metallurgical phases, which is a difficult task considering the complexity of the alloys. However, an approximation for the major fission products can be made if these products are partitioned and the following assumptions are made:

- Zr, Nb, and Mo are all in solution in the fuel phases.
- Alkali elements are dissolved to some extent in the bond sodium.
- The noble metals precipitate as compounds.
- The rare earths precipitate as a separate compound or alloy.
- The majority of the alkaline earths precipitate separately.

Post-irradiation examinations of high burnup fuel appear largely to support both this partitioning and these assumptions.

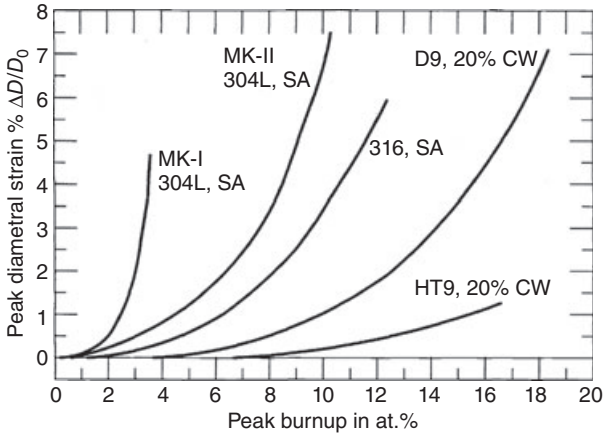

Fig. 29 Progressive improvement in cladding deformation (swelling and creep) of metallic fuel elements (EBR-II irradiations).

Tab. 2 Volume change due to major nonsoluble fission products.

Element group	*Fission yield per 100 fissions*	*State*	*Average molar volume ($cm^3\ mol^{-1}$)*	*Percent volume change per % BU[a)]*
Alkali (Cs, Rb)	22.2	Liquid, 70% in Na bond	70	0.108
Alkaline earth (Sr, Ba)	14.7	Solid, liquid, in precipitates and 20% in Na bond	20	0.146
Rare earths + Pd (Ce, Nd, etc.)	51.4	Solid, precipitates	20	0.792
(Tc, Ru, Rh, Ag)	23.3	Solid, precipitates	9	0.162
Total nonsoluble fission products				1.18

BU, burnup.
a) For a molar volume of 12.9 $cm^3\ mol^{-1}$ of U–19Pu–10Zr.

Another reason for partitioning these fission products is their different migration behavior in the fuel; such grouping allows an evaluation of this migration on the properties of the various radial phasal zones. The accommodation of the nonsoluble fission products predictably results in a volume expansion as a function of burnup. However, the U and Pu are removed from the lattice as they fission, which results in a volume decrease that partially offsets the volume expansion due to fission products. Further, it was assumed that all of the fission product Zr, Nb and Mo are soluble in the matrix, which in turn compensates for some of the volume decrease due to the disappearance of U and Pu from fissioning. Thus, nongaseous fission products contribute to the volume change in three ways:

1) A volume increase due to nonsoluble fission products.
2) A volume decrease due to the fissioning of U and Pu.
3) A volume increase due to the increase of Zr, Mo and Nb, which are soluble in the fuel matrix.

The result of the latter two contributions is estimated as follows: At 10 at.% U–Pu burnup, the average fuel matrix composition of U–19Pu–10Zr (wt%) changes from 77(U–Pu)23(Zr) at.% to 71(U–Pu)29(Zr–Nb–Mo) at.%, with an associated volume change of 0.2 vol.% per percent burnup.

As shown in Fig. 30 for a 17 at.% burnup U–19Pu–10Zr fuel sample, the rare earths are found to collect in two separate phases in primarily large pores towards the periphery of the fuel and in gaps between the fuel and cladding. Evidently, these elements migrate down the temperature gradient. While one of these two phases contains most of the Pu, the other noble metals are concentrated in blocky-type precipitates throughout the fuel. Mo, Zr and Nb are not found as separate phases, and are thus most likely retained in solution in the various fuel phases. A chemical analysis of the bond sodium indicated that a major fraction of the alkali, and also some of the alkaline earth elements, can simply be added to the bond sodium volume. The fuel volume changes due to these fission products are

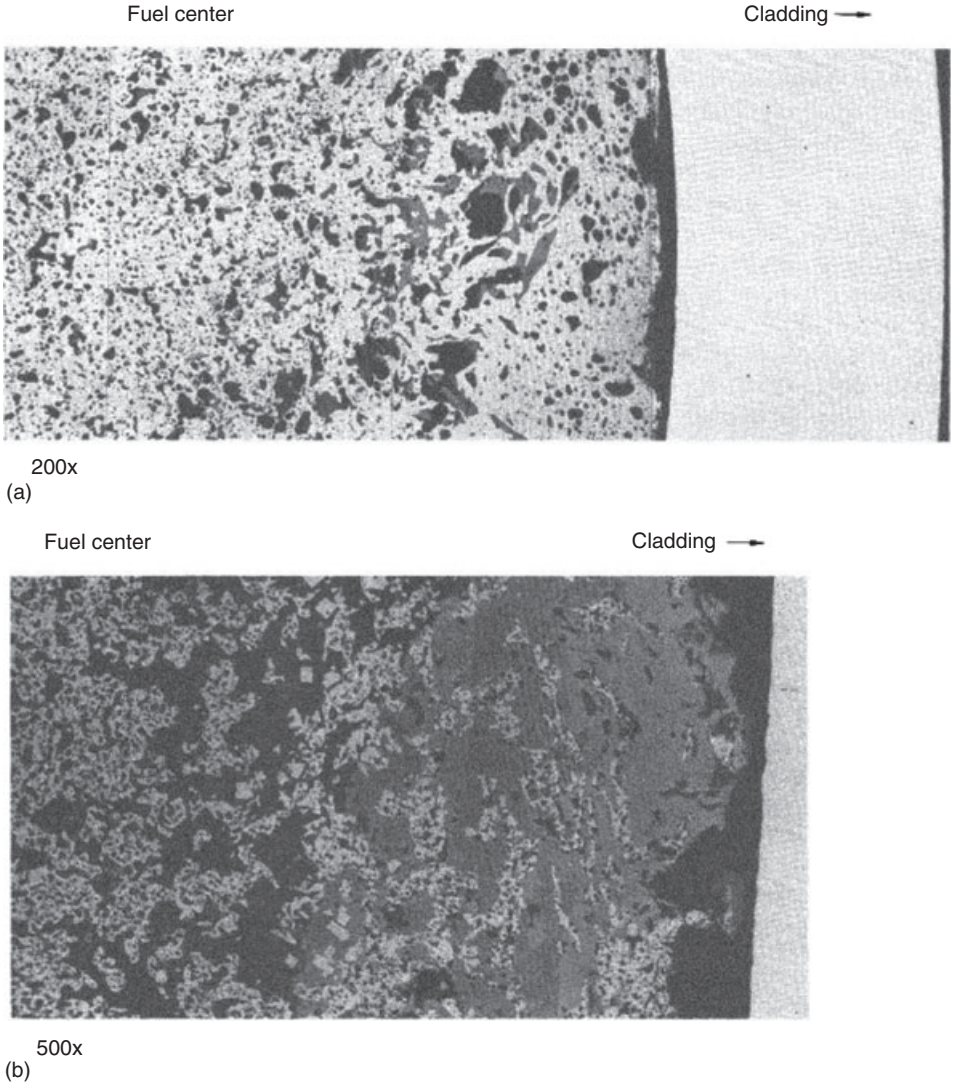

Fig. 30 (a) Radial strip across medium-burnup U–19Pu–10Zr element, showing lanthanide fission products that have migrated into the voids near the cladding. (b) A similar strip across a high-burnup U–19Pu–10Zr element showing large deposits of two different lanthanide alloys and blocky noble metal precipitates.

also listed in Table 1. The total volume of the nonsoluble fission products amounts to approximately 1.2% fuel volume increase per percent burnup.

It is interesting to compare these coefficients with more recent fission-enhanced creep data obtained for ceramic fuels, as listed in Table 4.

In addition, at any time during the irradiation a fraction of Xe and Kr does not find its way to the general porosity and thus resides in the fuel matrix. This

Tab. 3 Creep experiments on metal fuels.

Experimenter	*Year*	*Fuel*	*Method*	T_i	$F(\cdot 10^{12})$	σ *(MPa)*
Roberts Cottrell	1956	α-U	Spring	100	1	2–14
Hesketh	1968	α-U	Spring	180	1	9
Zaimovsky	1958	α-U	Tensile bar	250	2	2–150
Englander	1968	α-U–1.1Mo	Tensile bar	440	4	4
Konobeevsky *et al.*	1958	α-U–0.9Mo γ-U–9Mo	Bent foil	200	3	80–270

Tab. 4 Radiation-enhanced creep constants of various fuels.

Fuel	A $(\cdot 10^{-25})$	T/T_m	*References*
α-U	800	0.3	Hesketh (1968) and Zaimovsky (1958)
UO_2	8	0.25	Dienst (1977), Clough (1970), and Solomon (1973)
MOX	56	0.25	White (1999)
UC	1	0.3	Clough (1977)
UN	2	0.3	Brucklacher and Dienst (1971) and Zeisser *et al.* (1977)
U–10Mo	500	0.3	Kim *et al.* (2012)

gas is in solution and in very small precipitates in a solid, liquid or high-pressure gaseous state. Moreover, this fraction of resident gas is probably very different in the various fuel phases and has not been well characterized. Nonetheless, post-irradiation data, including a wet chemical analysis of high burnup irradiated fuel, have indicated that an average value of 10% of the gas volume for an entire element is a reasonable estimate. Such a fraction in solution and in liquid–solid or non-ideal dense gas amounts to ~0.2% fuel volume increase per percent burnup. This brings the total volume increase to approximately $(-0.2 + 1.2 + 0.2) = 1.2\%$ per percent burnup.

As a result of this volume increase, and assuming that no cladding deformation occurs, an as-built smeared density of 75% would change to 81% at 10 at.% burnup, and to 90% at 20 at.% burnup, respectively. It appears that, in this high burnup range, the initially open porosity would become increasingly closed-off and the fission gas pressure in the fuel would build up more rapidly, as less generated gas would be vented to the plenum. In effect, this would represent the onset of a possibly significant FCMI, although in irradiations with 75%-smeared-density fuel FCMI has not been observed up to 18% burnup.

This is readily explained for austenitic stainless steel claddings such as type 316 and D9. As shown in Fig. 30, cladding deformation at high burnup in these steels is so large that it compensates for any solid fuel volume increase. Deformation in type 316 and D9 cladding is caused mainly by swelling, and any irradiation creep strain can be accounted for by plenum pressure alone; hence, there is no evidence of FCMI.

Because of the desire to reduce cladding deformation at high burnup (or fluence), a nonswelling martensitic stainless steel, HT-9, is the current cladding material of

choice for LMR fuel elements. As shown also in Fig. 30, the deformation at 16 at.% burnup is only approximately 1%, and the fuel smeared density at this point should have changed from 75% to approximately 85%. Apparently, little FCMI has occurred at this burnup, even with the nonswelling material, as the cladding creep strain can be accounted for by plenum pressure only, within the accuracy of the calculations. In order to evaluate the effective smeared-density value at which significant FCMI does occur, HT-9-clad fuel elements with an initial fuel smeared density of 85% were irradiated along with the usual 75% (Tsai, 1991). The resulting cladding strains are compared in Fig. 31. It is clear that the rate of cladding strain has increased for the initially 85% fuel smeared density elements, somewhere prior to 12 at.% burnup, when solid fission products increased the fuel smeared density from 85% to approximately 95%. It appears from these data that FCMI became substantial in this interval, although even for initial values of 85%, open porosity apparently develops to some extent, and substantial albeit less gas release occurs, as is also shown in Fig. 32. Only when solid fission products increase the fuel smeared density to well above 85% does FCMI become clearly evident. It may be concluded that, even with nonswelling cladding, significant FCMI can be avoided to high burnup if the as-built fuel smeared density is kept to 75%. In this discussion, it has been assumed that the fuel porosity is uniformly affected by the accumulation of fission products. However, it is clear that, based on the observed porosity patterns and the positioning of fission products in the fuel, this may be too simplistic for a proper evaluation of FCMI.

In order for the pressure in the closed porosity to be transmitted to the cladding, the fuel alloy itself has to deform plastically. This is easily envisaged for fuel at high temperatures, such as exist in the center region of a fuel element. However, as discussed in the following section, fission-induced creep provides a deformation mode also at low temperatures.

3.1.1 Fission-Induced Creep

Stress in the cladding due to fuel swelling will thus also depend on the effective creep rate of the fuel in-reactor. Measurable creep deformation of α-U during fissioning at temperatures where classical creep does not

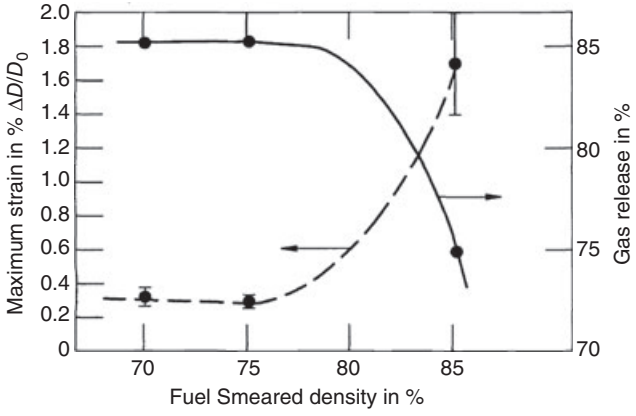

Fig. 31 Peak cladding diameter increase and gas release fraction of HT-9 clad U–9Pu–10Zr fuel of various as-built smeared densities, at 12.5 at.% burnup (Tsai, 1991).

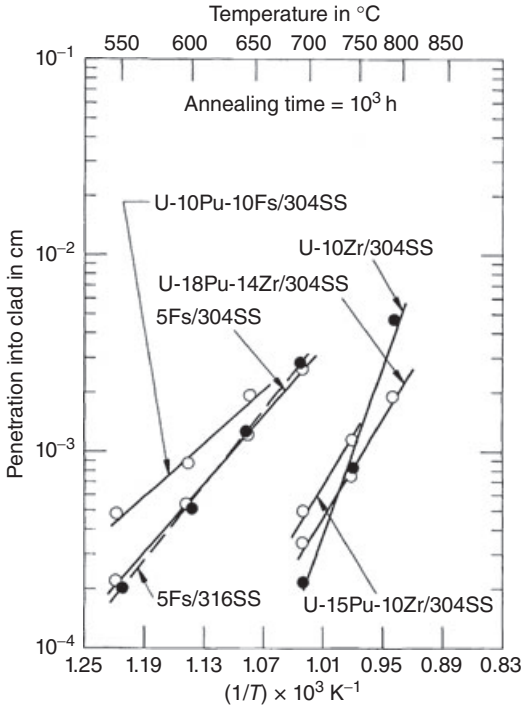

Fig. 32 Depth of interaction layer in cladding for various fuel–cladding diffusion couples (Zegler and Walters, 1967).

occur was first demonstrated by Roberts and Cottrell (1956). These researchers measured the stress relaxation of pre-loaded U springs under irradiation. The first comprehensive study was performed by Zaimovsky (1959), who used tensile bars of U in an instrumented irradiation. These studies clearly established that at low temperature, the in-reactor creep rate, $\dot{\varepsilon}$, of U, is independent of temperature and linearly dependent on both stress, σ, and fission rate, F; that is:

$$\dot{\varepsilon} = A \cdot \sigma \cdot F \ \ldots \qquad (4)$$

where the creep coefficient, A, is in units of $cm^3\ MPa^{-1}$.

The results of very few studies on uranium alloys have been published. Englander and Montpreville (1968) measured the creep rate of U-1.1 wt% Mo, while Konobeevsky *et al.* (1958) measured that of both 0.9 and 9 wt% Mo (the latter is the only experiment performed with a γ alloy). The experiments on metallic fuels are summarized in Table 3. Konobeevsky's experiment, which was performed with clamped pre-bent foils, was a stress–relaxation experiment and the data were not analyzed to yield a creep coefficient. A recent analysis of in-reactor deformation of U-10Mo foils by Kim *et al.* (2012) yielded a creep coefficient of $500 \times 10^{25}\ cm^3\ MPa^{-1}$.

3.2 Fuel–Cladding Chemical Interaction

FCCI in an all-metallic fuel element is in essence a complex multicomponent

diffusion problem. The characterization of fuel-cladding interdiffusion is exceedingly difficult because of the number of alloy components involved. With stainless steel cladding, even in the most simple fuel alloys such as U–Fs and U–Zr, at least five major constituents participate in the diffusion process. In addition, minor alloy components such as C, N and O, as well as fission products – particularly at higher burnup – appear to play an important role. The potential problem of interdiffusion of fuel and cladding components is essentially twofold: (i) a weakening of the cladding's mechanical properties; and (ii) the formation of relatively low melting point compositions in the fuel. In an attempt to assess the severity of these two deleterious effects prior to irradiation testing of specific fuel elements, diffusion couple experiments are customarily performed in the laboratory.

During the 1960s, ANL tested a large number of fuel–cladding combinations with this diffusion method. It was concluded that the 300 series of austenitic stainless steel cladding has an acceptable degree of cladding attack for U–Fs fuel. However, the addition of Pu increased the rate of attack and, more importantly, decreased the temperature at which melting was observed in the diffusion zone. As shown in Fig. 32 and Table 5 (Zegler and Walter, 1967), a marked improvement in both diffusion rates and minimum melting temperature was obtained through the addition of at least 10 wt% Zr in the fuel alloys, whereas Ti, which was also considered as a fuel alloy addition, proved to be ineffective. This discovery forms the basis for the selection of 10 wt% Zr alloys for the present IFR fuels.

Tab. 5 Melting temperatures from diffusion couple data after 300–700 h at temperature.

	T_m (°C)			
Cladding	*304*	*316*	*HT-9*	*D-9*
U–8Pu–10Zr	>760	790	740	<750
U–19Pu–10Zr	>780	790	>780	>730
U–26Pu–10Zr	—	<775	650	650
U–15Pu–11Zr (1967)	>800	>800	>800	>800

Considerable variability in cladding attack was observed with U–18Pu– 14Zr; for example, type 310 showed a depth of 30–44 µm after 5000 h at 750 °C (similar to type 304), while type 309 showed a depth of less than 8 µm. However, in none of these combinations did melting occur after 5000 h at 800 °C (Zegler, 1967). It was concluded that the variability in cladding attack was due to the formation of thin layers of oxygen-stabilized Zr, which formed at the original fuel–cladding interface. These layers acted as diffusion barriers, and the extent of their formation would depend on the oxygen activity in the stainless steel, which could vary from type to type. It is of interest to note the limited test results then obtained on ferritic type 440 stainless steel because of the current use of ferritic–martensitic cladding. Diffusion tests with U–10Pu–14Zr and this ferritic steel showed molten phase formation at 750 °C after only five days. This inferior behavior, compared to austenitic steels, led to the ferritic steels being further considered during the 1960s.

These results and earlier data reported by Kittel (1949) on diffusion experiments with uranium (see Fig. 33) also led the research groups to conclude that Ni played an important role in fuel–cladding interdiffusion. These findings and conclusions are relevant to the newly developed low-swelling cladding materials used for the IFR fuel elements.

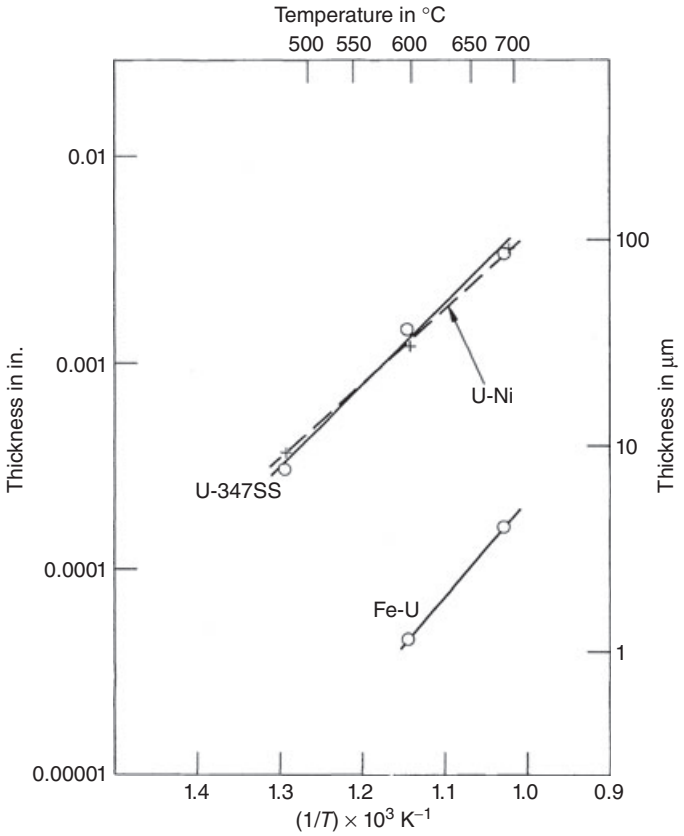

Fig. 33 Thickness of interaction layers in diffusion couples after six-day annealing period (Kittel, 1949).

The austenitic cladding D-9 contains Ti, which forms extremely stable compounds with interstitial elements in the steel, rendering these elements unavailable for the possible formation of a Zr-compound diffusion barrier. On the other hand, the martensitic steel HT-9 contains very little Ni and might be expected to behave like the aforementioned type 440 stainless steel.

In order to specifically assess the propensity for molten phase formation, diffusion experiments were performed with the current IFR fuel–cladding combinations. Series 300 stainless steels were included, as well as fuel samples from an archive fuel element that was fabricated in 1967 for comparison with the previous experiments. The results of these experiments are summarized in Table 5. These are "consistent" with the 1960s data, in that there is considerable scatter in both sets of data with regards to the various fuel/cladding types, but within the same wide range of results.

The results of this type of testing have highlighted many indications as to the influence of the formation of a surface layer of zirconium containing 20–30 at.% of interstitial elements (O, N, C), as was found in the 1960s studies (when oxygen was thought to play a dominant role). The interstitial element found in greatest

abundance in the interface zirconium layers in recent studies (Hofman *et al.*, 1986) was nitrogen. Moreover, it seemed that thicker layers were formed in couples where the nitrogen content of the cladding alloy was greatest. Hence, it was speculated that the enhanced compatibility of the 316 couples, compared to the D9 and HT9 alloys, was due to the 600 ppm N_2 content versus 40–50 ppm in the HT9 and D9 alloys. The increased C content was apparently not effective in enhancing HT9 compatibility compared to the 316 and D9 austenitic alloys, perhaps due to carbide stability at $T > 700\,^{\circ}\mathrm{C}$.

Another indication of the effect that nitrogen has on interdiffusion is that none of the diffusion couples containing the 1967 archive fuel showed any evidence of melting at the highest test temperature of 810 °C, and that they had formed much thicker Zr layers at the fuel–cladding interfaces. While the carbon and oxygen content of the various fuel alloys used in the test was similar, the nitrogen content of the 1967 vintage fuels was ~500 ppm by weight, compared to ~20 ppm by weight in the current IFR fuel alloys.

Subsequent studies were performed to show that the presence of small amounts of nitrogen (in a heat-treatment atmosphere) can induce the formation of Zr-rich layers on the surface of samples. These layers were then shown to enhance compatibility in subsequent diffusion–couple tests and appeared to be effective interdiffusion barriers. The relationship of how the layers form as influenced by the test technique, sample preparation, and so on, may also explain some of the scatter in the diffusion–couple data.

Metallographic examinations of the various diffusion couples led to the following general observations (Hofman *et al.*, 1986). A Zr layer containing approximately 20 at.% N is first formed at the interface of all fuel–cladding combinations, as shown in Fig. 34. This layer is thicker and apparently forms more readily in the case of type 316 stainless steel, which has a rather high dissolved nitrogen concentration. Subsequently, primarily Fe and Ni (in austenitic steels) diffuse into the Zr layer and form two distinct phases that also contain some U and Pu, indicating that

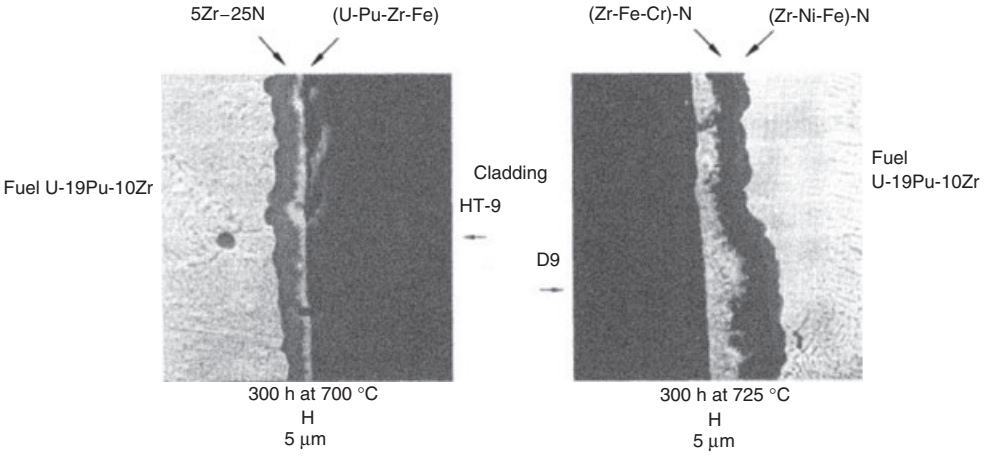

Fig. 34 Layers formed at fuel–cladding diffusion couple interfaces.

these elements can diffuse through the Zr compounds (see Fig. 33). Finally, further diffusion of U and Pu leads to the formation of fuel–cladding component phases equivalent to U_6Fe and UFe_2 on the cladding side of the Zr compound layer. In the case of austenitic steels, the UFe_2-type phase forms a "finger"-like diffusion front, a structure that is often observed in multicomponent diffusion when two of the diffusing species (in the present case, Ni and U) diffuse by a relatively rapid exchange mechanism (Van Loo *et al.*, 1984). The U_6Fe-like phase forms directly behind the "fingers" (see Fig. 35).

The interdiffusion zone is essentially the same for type 316 and D9 stainless steel, but the rate of formation is much lower for the former, due to the difference in the initially formed Zr–N layer. In the case of basically Ni-free ferritic steel, HT-9, the U_6Fe- and UFe_2-type phases form a single zone without the finger-like structure (also shown in Fig. 25). There exists a eutectic composition between these two phases, the temperature of which depends

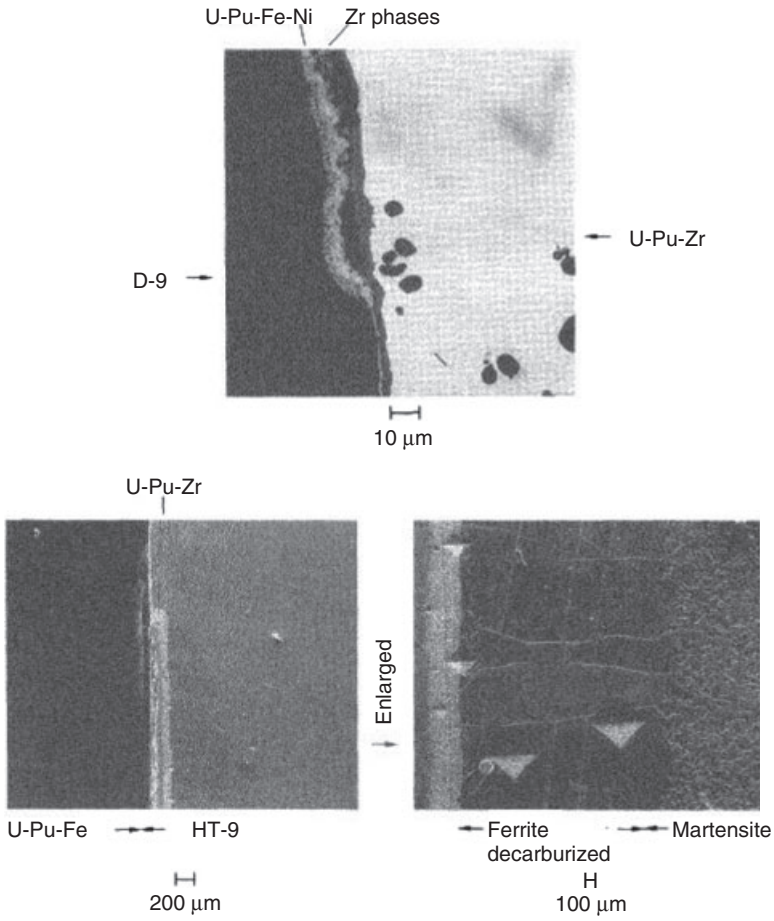

Fig. 35 Interaction layers formed after 300 h at 705 °C between (a) D9 steel and (b) HT-9 (left image) and U–19Pu–0 Zr fuel (right image). Note the decarburization in HT-9.

on the concentration of Pu, Ni and Zr in the phases, as well as U and Fe. However, judging from the data in Table 5 for D9 and HT9, this temperature appears to lie in the vicinity of the U–Fe eutectic of approximately 720 °C. Presumably, the type 316 stainless steel would have yielded a similar melting temperature had the test run for longer – that is, more U diffusion through the Zr layer would have occurred. As it were, melting in the case of type 316 or 304L occurred near 800 °C and appeared to have started in the fuel side of the diffusion couple. At this temperature, the diffusion of Fe and Ni into the fuel, rather than of U into the steel, leads to eutectic formation. The eutectic temperature in the Fe–U–Pu–Zr system drops significantly with Pu concentration, which may explain the lower melting temperatures for the 26 wt% Pu fuel. The melting in this case also started in the fuel side of the diffusion couple.

The results obtained with diffusion couples indicate what might occur in a reactor during FCCI. However, post-irradiation examinations and annealing experiments with irradiated fuel and cladding have shown significantly different behaviors of FCCI in an actual fuel element. The emphasis in the preceding discussion of the diffusion couple test has been in the formation of liquid phases, but except during possible transient events the fuel elements operate by design below these melting points. During normal operation, the FCCI is thus characterized by solid-state interdiffusion. As suggested earlier, Ni appears to play an important role in FCCI, with the preferential diffusion of Ni into the fuel resulting in a ferritic layer in the cladding of all austenitic steel–fuel combinations. This Ni, as well as some Fe, diffuses into the fuel to a depth several times as large as the Ni-depleted layer in the cladding. The ferritic layer, on the other hand, contains little or no fuel. The interdiffusion zone in a high-burnup U–5Fs 304L-clad element (Hofman, 1980) is very similar to those reported by Zegler and Walter (1967) in diffusion studies with the same fuel–cladding combination. A selection of post-irradiation observations (as listed in Table 6) shows some interesting differences various fuel–cladding combinations. For example, the Ni depletion in type

Tab. 6 Comparison of Ni-depleted (ferritic) zones in fuel–cladding combinations.

Fuel	*Cladding*	*Ni-depleted zone[a)] (μm)*	*BU (at.%)*	*BOL T (°C)*	*Ce–Nd (at.%)*	*DPH*
U–5Fs	304L	50 (10)[b)]	10	560	~0	230
	316	10 (10)[b)]	10	560	~0	nm[c)]
U–15Pu–9Zr	304L	140	5	650	Few	280
	316	30	5	650	Few	280
U–9Pu–10Zr	D9	100	17	580	~20	1050
	316	70	13	580	nm[c)]	1000
U–10Zr	D9	20	17	580	nm[c)]	nm[c)]
	HT-9[a)]	100	5	650	3	200
U–19Pu–10Zr	HT-9	45	12	600	—	350

BOL, beginning of life; DPH, diamond pyramid hardness.
a) Decarburized zone for HT-9.
b) Extrapolated from Zegler and Walters diffusion couples.
c) Not measured.

316 stainless steel is substantially lower than in type 304 for both U–5Fs (Hofman *et al.*, 1976) and U–Pu–Zr (Murphy *et al.*, 1969), whereas Zegler and Walter found no difference between these two steels in their diffusion studies. Moreover, a difference in the radiation-enhanced diffusion of Ni in the two steels does not explain this different behavior. The effect of rare earth fission products on Ni diffusion was considered because these elements are found in the Ni-depleted zone of austenitic steel-clad U–Pu–Zr fuel elements up to a concentration of a small percentage at 5 at.% burnup (see Fig. 36 and Table 6), and to as much as 20% in the high-burnup D9-clad elements, as illustrated in Fig. 37 (this is also reflected in the hardness of the Ni-depleted zone). Rare earth fission products of the lanthanide series migrate readily to the cladding in Pu-containing fuel (as shown in Fig. 30), but not as easily in U–Zr, which might explain the large difference in layer width between those fuels and D9 cladding. However, there are no rare earth elements found in the Ni-depleted layers in the U–5Fs fuel, yet the difference between type 316 and 304L is of the same order as that of U–15Pu–9Zr fuel.

There is no satisfactory explanation of this behavior at this point, other than the suggestion that the aforementioned

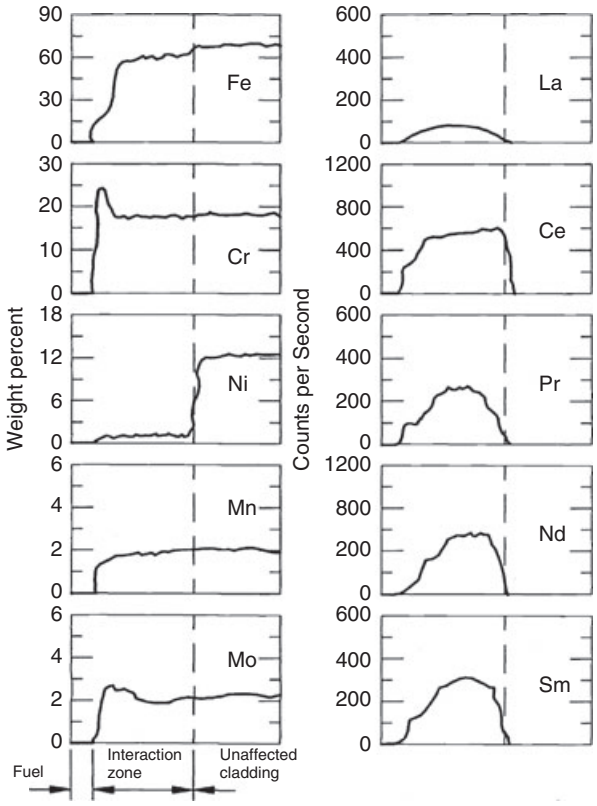

Fig. 36 Electron microprobe scan of interaction zone at U–Pu–Zr-type 316 cladding interface showing Ni depletion and lanthanide penetration (~5 at.% burnup at 640 °C cladding temperature).

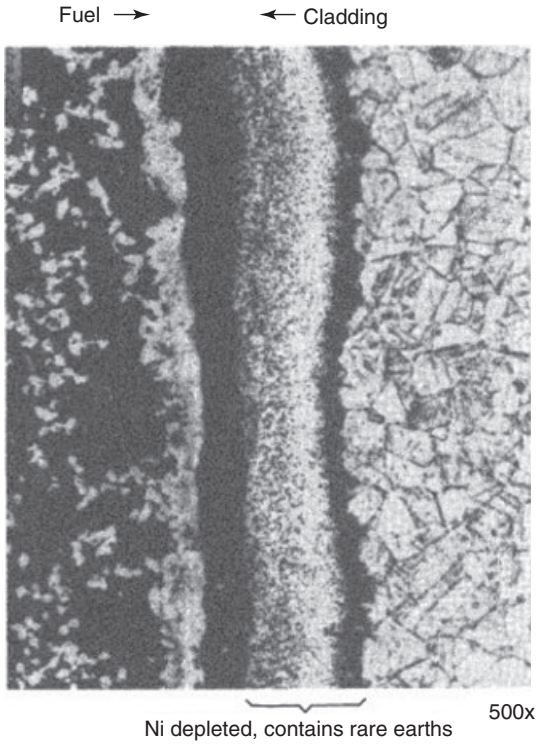

Fig. 37 Micrograph of etched cross-section showing fuel–cladding interdiffusion of U–Pu–Zr and D-9, in pile, after ~12 at.% burnup at ~500 °C.

initial Zr-rich layer formation at the fuel–cladding interface of the various fuel–cladding combination is sufficiently different, and is affected differently enough during irradiation to alter Ni diffusion from the cladding.

FCCI between austenitic and martensitic steel has both similarities and differences. Because HT-9 contains very little Ni, depletion of this element – which seems to control FCCI in austenitic D9 – does not apply to HT-9. However, the ferritic layer in D9 formed by Ni depletion is essentially similar to a ferritic layer in HT-9 that results from decarburization of the original martensite. An example of this is shown in Fig. 38. Such decarburization and ferrite formation, it may be recalled, also occurred in the diffusion couples illustrated in Fig. 37. However, the differences in FCMI between austenitic and martensitic steel may be more significant than the aforementioned similarity. First, the rate of ferrite formation due to decarburization of HT-9 is lower than that due to Ni depletion in D9 at comparable temperatures. Moreover, the diffusion of rare earths into the ferritic layers is quite different for the two steels. Unlike the uniform diffusion in D9, rare earths diffuse only partially along a uniform front, but rather more along grain boundaries in HT-9, as shown also in Fig. 40.

Although the present understanding of FCCI is not complete at this juncture, it would appear that the data allow the

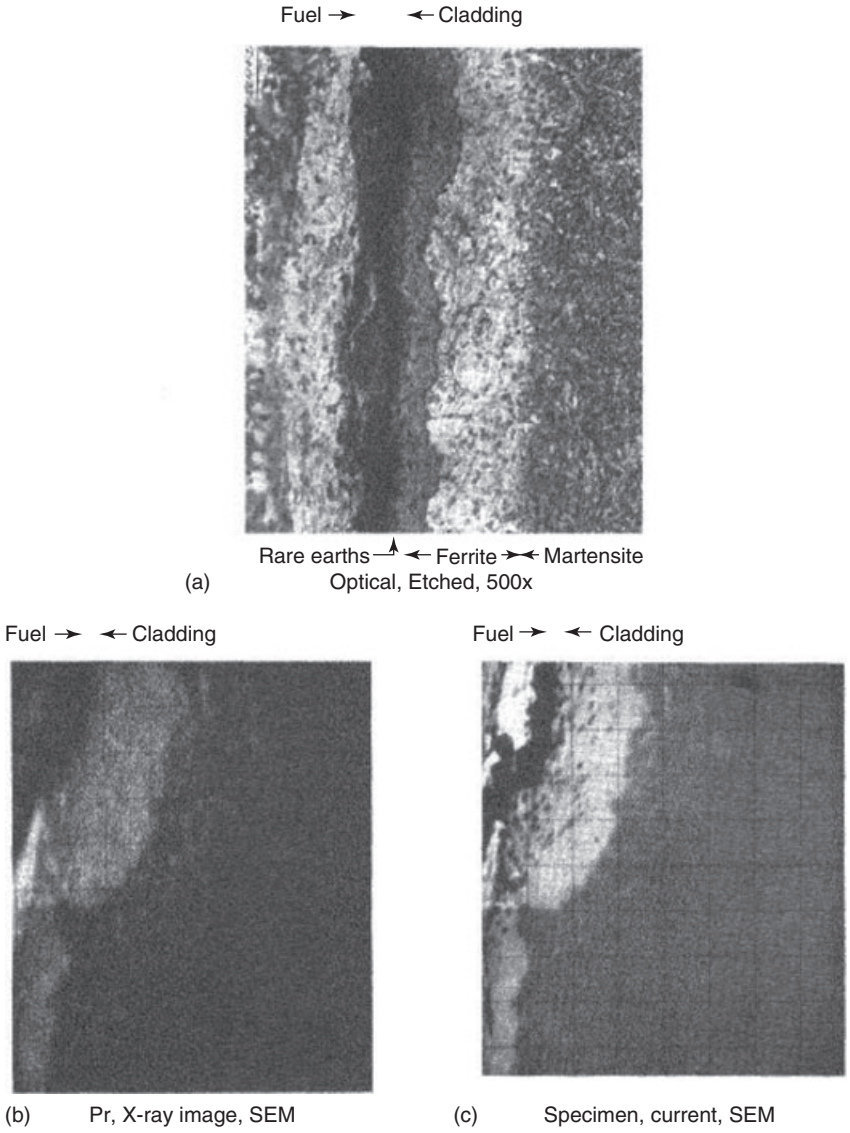

Fig. 38 (a–c) Fuel-cladding interdiffusion of U–10Zr and HT-9 (in-pile) after 6 at.% burnup at ~620 °C.

following general observations to be made. Prior to the accumulation of significant amounts of lanthanide fission products at the fuel–cladding interface, FCCI depends on the particular fuel–cladding combinations; that is, various degrees of Ni depletion in austenitic cladding and decarburization of martensitic cladding have a solid-state diffusion-type time and temperature dependence. Although lanthanides ultimately control FCCI, their presence at the internal cladding surface depends not only on burnup but also very strongly on their radial migration in the

fuel. Although radial lanthanide migration increases with fuel temperature for all fuel alloys, it is most rapid in U–Pu–Zr, less so in U–Zr, and least in U–5Fs.

The *in-situ* formation of Zr–N layers in diffusion couples, and the reduced Ni depletion found in type 316 stainless steel, indicate the feasibility of improving the FCCI. However, the FCCI problem with austenitic cladding might be largely academic, since swelling alone renders these steels unacceptable for use at high burnup. High-burnup operation requires a low-swelling cladding material such as HT-9, and consequently an acceptable FCCI is more important in this steel.

Although melting due to FCCI is not expected at normal fuel element operating conditions, the ex-reactor diffusion tests indicate that liquid phase formation needs to be considered if cladding temperatures were to reach the 700–800 °C range during transient conditions. In these considered transients, the higher temperatures in this range are reached in events that last only for minutes, whereas relatively lower temperature events such as a loss of coolant combined with a disabled heat rejection system may last for many hours. In order to better characterize liquid phase formation in cladding and fuel at elevated temperatures, sections of various irradiated fuel elements have been heated in an in-cell apparatus over a range of temperatures and times (Tsai, 1990). These studies showed no evidence of liquid phase formation below ~725 °C for test durations of up to 7 h, which was in general agreement with the diffusion experiments discussed above, but yielded a large body of kinetic data at higher temperatures (Tsai, 1991). Figure 39 shows an envelope of test results on several fuel–cladding combinations measured as a function of time at 800 °C. The broadness of the data range is due to the number of fuel–cladding combinations tested; that is, 0–26% Pu and type 316, D-9 and HT-9 steels, as well as various burnup levels and irradiation conditions of the tested samples. Further testing is still in progress.

In general, the penetration depths appears to be parabolic functions of time with a power of less than 1. The rate of attack is similar for HT9 and D9, but generally lower for type 316 with all fuel compositions. It is interesting to note that for the parameter range covered thus far in

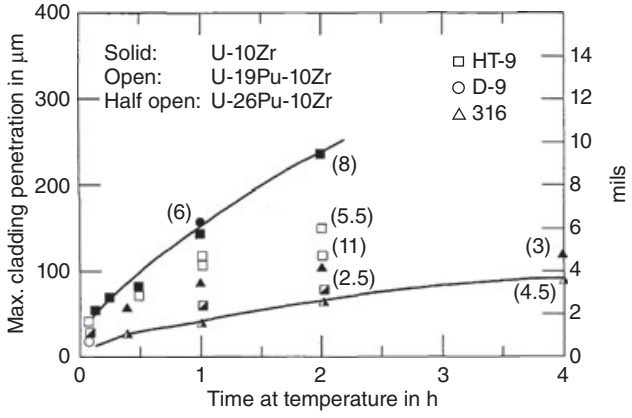

Fig. 39 Envelope of fuel–cladding penetration depth as a function of time at 800 °C during post-irradiation heating tests. The burnup times of the test samples are shown in parentheses (Tsai, 1991).

these post-irradiation heating tests, 0% Pu fuel has shown the highest rate of attack and 26% Pu fuel the lowest, opposite to the trend observed in diffusion couples. A metallographic examination of these post-irradiation samples revealed that the FCCI is similar to that observed in unirradiated diffusion couple tests, with the exception of a pronounced effect of rare-earth fission products in high-burnup fuel samples. This experimental program has not advanced to development of a satisfactory fundamental model for the observations. Meanwhile, correlations of cladding penetrations with temperature and time derived from these preliminary test results are being used to evaluate the transient behavior of metallic fuel elements.

4 Transient Testing

A series of experiments was performed at the transient reactor test facility (TREAT) between 1984 and 1987 (Bauer and Wright, 1990). The aim of these experiments was to study cladding failure thresholds and other safety-related fuel behaviors during simulated transient overpower (TOP) accidents.

The data needs specifically addressed by these tests were as follows:

1) To determine the margin of failure and identify the underlying mechanisms.
2) To assess prefailure axial expansion as a potentially significant prefailure reactivity removal mechanism.
3) To preliminarily assess post-failure events, that is, the behavior of the disrupted fuel and coolant.

For the IFR experiments, preirradiated fuel was tested. Each test pin in this series was subjected to similar over-power conditions in a simulated TOP accident, namely a full coolant flow and an exponential power rise over 8 s.

Simple models of prefailure expansion and cladding failure were developed and validated. While the safety-related fuel behavior of all fuel types tested was similar, fission gas retention and melting point were found to account for the observed differences. The prefailure axial expansion in irradiated fuel was always positive and significant beyond thermal expansion. Large expansions at low burnups were measured in U–Fs fuel, but not in IFR-type fuel. At medium to high burnup, expansions in the range of 2–4% were typical of all fuels tested. The expansion of fission gas trapped in the melting fuel provides a basis for modeling axial expansions, and differences in the amounts of dissolved gas account for measured expansion differences between fuel types. The cladding failure threshold with the 8-s over-power was fourfold the nominal power over a wide range of burnups and fuel types tested. From the data base generated thus far, successful cladding failure models should include effects of both overpressure and penetration of cladding by low-temperature molten phases. Because rapid cladding penetration by molten phases also requires extensive fuel melting, failure might be delayed somewhat in a fuel with a high melting point, such as U–10Zr.

Studies with the present cladding failure model have indicated that, for the fuel burnups and heating rates employed, pins fail at or near the threshold point of rapid eutectic penetration. However, different modeling issues and questions arise concerning slower cladding damage rates at lower temperatures; extending the model validation into these areas requires that

higher burnup fuel be tested and the test fuel be overheated to lower temperatures for longer times.

Post-failure disruption in all fuel types tested involved a benign ejection of the failed fuel element's inventory of molten fuel through a small local breach at the top of the fuel. Extensive disruption of the solid fuel remaining within failed fuel elements is possible if a significant amount of fission gas is dissolved in that fuel. Once ejected, molten fuel was highly mobile in the coolant channel, showing little tendency to cause blockages.

The TOP experiments performed at TREAT provided no confirmation of the analysis of longer-term transients, such as a loss of coolant events. In order to test the combined effect of liquid-phase cladding penetration and internal gas pressure, irradiated elements were tested in an in-cell furnace in a programmed manner (Liu *et al.*, 1990).

To date, three irradiated metallic fuel elements have been tested in a whole-element apparatus at a peak temperature of 800 °C, in which the axial temperature profile along the test elements duplicated the in-reactor conditions. Prior to these tests, the time of cladding breach was predicted by both the steady-state fuel element modeling code LIFE-METAL and the transient code FPIN2 (Billone *et al.*, 1986; Kramer and Bauer, 1990). An important and necessary aspect of the code prediction was the empirical correlation used for liquid-phase cladding penetration, which was derived from the in-cell heating tests on irradiated fuel samples discussed above. Both of these codes closely predicted the time of cladding breach, thus validating the approach used to determine cladding stress and the use of stress–rupture correlations. Post-test examinations of the breached fuel elements also showed fuel axial expansion due to retained fission gas (Tsai, 1991).

5 Operation of Fuel Elements with Breached Cladding

Unlike oxide fuel, metallic fuel is chemically compatible with the sodium reactor coolant, which is why sodium is used as a thermal bond between fuel and cladding. Of course, sodium coolant is not expected to react with metallic fuel if, for some reason, a cladding breach occurs. The behavior of failed fuel elements during continued operation is thus governed by the properties of the fuel, its fission products, and the cladding, and is not affected by any fuel–sodium reaction.

Several so-called run-beyond-cladding breach (RBCB) tests have been performed in EBR-II with U–Fs, U–Zr, and U–Pu–Zr fuel clad with type 316, D9, and HT9 stainless steels (Batté and Hofman, 1990). The purpose here was to confirm the expected benign behavior of metallic fuel elements during RBCB operation, and to characterize the release of fission gas, delayed neutron (DN) emitters, and possibly fuel from breached elements. Some pertinent parameters and results of these tests are summarized in Table 7.

In order to simulate cladding failures prior to the designed end-of-life of an element, an area on the cladding of a preirradiated element is machined down to approximately 25–50 μm. Shortly after reinsertion in the reactor, cladding failure occurs in this thinned area, an event that is annunciated by both fission gas and DN signals on the reactor monitoring system. A typical pattern of these signals is shown in Fig. 40. The pattern consists of a short DN signal that coincides with the expulsion

Tab. 7 Summary of RBCB tests with metal fuel in EBR-II.

Experiment	*XY-21A*	*XY-24*	*XY-27*	*X482*	*X482A*	*X482A*
Composition (wt%)	U–5Fs	U–19Pu–10Zr	U–19Pu–10Zr	U–19Pu–10Zr	U–10Zr	U–19Pu–10Zr
Cladding material	316SS	316SS	316SS	D9	D9	HT9
Final BU (at.%)	~9.3	~7.5	~6.0	14.4	13.5	13.5
Days RBCB	54	233	131	168	100	150
DN signal[a] (s^{-1})	~30–40	[b]	[b]	~600	~700	[c]
Weight loss (g)[d]	2.0	2.7	2.5	4.0	3.6	3.9
Peak cladding temperature (°C)	550	550	550	600	600	600

a) Counts above background.
b) Unavailable due to malfunction of instrument sensitivity.
c) None detected, breached at startup.
d) Expulsion of bond sodium + fission gas + cesium accounts for the weight loss; fuel loss was negligible.

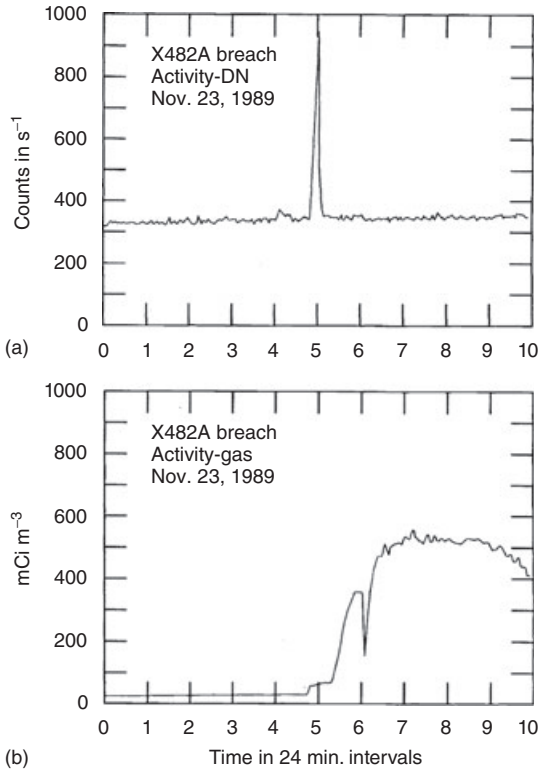

Fig. 40 (a) Delayed neutron (DN) and (b) fission gas signals observed on cladding breach of a high-burnup metallic fuel element in EBR-II.

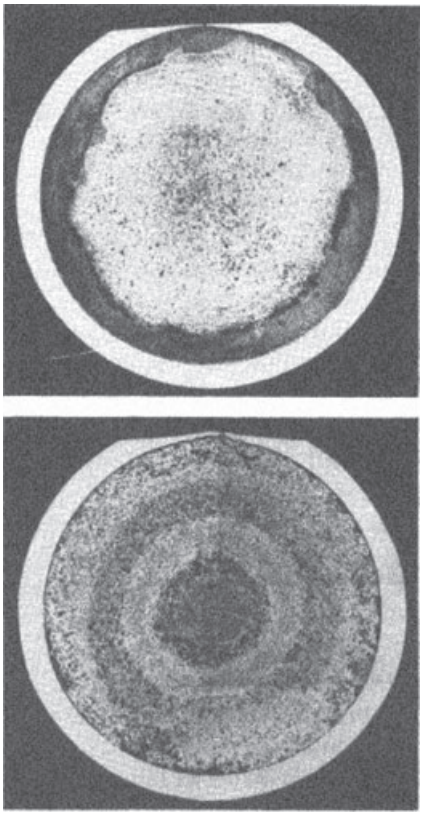

Fig. 41 (a,b) Metallographic cross-sections through cladding breaches of several metallic fuel elements after extensive run beyond cladding breach (RBCB) operation (the flat section on the cladding was machined to induce failure).

of bond sodium through the breach. When the bond sodium is gone, the transport of DN precursors to the breach site is slowed down enough to essentially decay before reaching the reactor coolant. A large portion of ^{133}Cs is expelled with the bond sodium, as reflected in a corresponding increase of this fission product in the reactor coolant.

Most of the long half-life fission gas that has collected in the element during its preirradiation is also released in a short period following cladding breach, and this results in a virtually complete depressurization of the element. The long-term release is characterized by measuring fission gas isotopes as they are produced during the RBCB operation.

Because the element is depressurized, and because FCMI is insignificant – either from the fuel itself or from the lack of fuel–sodium reaction – there is little or no cladding stress during RBCB operations, particularly with high-swelling austenitic cladding. As a result, the cladding breach size remains small (as shown in Fig. 41a), even after approximately 100–200 days of operation of the elements in the breached mode. A similar RBCB exposure within HT-9-clad elements exhibited more crack extension and widening (see Fig. 41b). This may indicate a certain amount of FCMI resulting from trapped fission gas in closed-off porosity (see Section 3.1). This trapped gas also causes the fuel to swell somewhat at the breach site but no fuel was extended through the breach even after 150 days of RBCB operation.

Because of the expulsion of the bond sodium from breached elements, the fraction of sodium logged in the open fuel porosity also disappears, and the thermal conductivity of the fuel slug, which had increased upon sodium logging, returns to a value commensurate with a low-pressure gas-filled porosity. The main effect of the resulting increase in fuel temperature appears to be an enhanced rare earth fission product transport to the periphery of the fuel slug, and an increase in FCCI. The depth of rare earth penetration into the cladding at the top of the fuel after 150–200 days of RBCB operation is approximately twice that in unbreached elements at comparable burnup and cladding temperature. This provides further indication that the behavior of rare earth fission products plays an important role in FCCI.

References

Angerman, C.L. and Caskey, G.R. (1964) *J. Nucl. Mater.*, **13**, 182.

Barnes, R.S. (1958) Proceedings of the 2nd United Nations International Conference on Peaceful Use of Atomic Energy, vol. 5, p. 500.

Barnes, R.S. (1964) *J. Nucl. Mater.*, **11**, 135.

Batté, G. and Hofman, G.L. (1990) Proceedings of the International Conference Fast Reactor Safety, Snowbird, UT, August 12–16, p. 207.

Bauer, T.H. and Wright, E. (1990) *Nucl. Technol.*, **92**, 325–352.

Beck, W.N. (1968) Report ANL-7388, Argonne National Laboratory.

Beck, W.N. and Foussek, R.J. (1969) *Trans. Am. Nucl. Soc.*, **12**, 78–79.

Bellamy, R.G. (1962) Institute of Metals Symposium on Uranium and Graphite, London, UK, Paper No. 8.

Betten, P.R. (1985) *Trans. Am. Nucl. Soc.*, **50**, 239–240.

Billone, M.C., Liu, Y.Y., Gruber, E.E., Hughes, T.H., and Kramer, J.M. (1986) Proceeding of the International Conference Reliable Fuels for Liquid Metal Reactors, pp. 5–77.

Blake, L.R. (1961) *Reactor Sci. Eng.*, **14**, 31.

Bleiberg, M.L., Jones, L.J., and Lustman, B. (1959) *J. Appl. Phys.*, **27**, 11.

Blumenthal, B., Sanecki, J.E., Busch, D.E., and O'Boyle, D.R. (1969) Report ANL-7259, Argonne National Laboratory.

Brucklacher, D. and Dienst, W. (1971) *J. Nucl. Mater.*, **36**, 244–247.

Buckley, S.N. (1961) in: *Properties of Reactor Materials and the Effects of Radiation Damage*: Littler, D.J. (ed.), Butterworths, London, p. 413.
Buckley, S.N. (1966) Report AERE-R5262, UK Atomic Energy Authority.
Burris, L. (1986) *Chem. Eng. Prog.*, **83**, 35–39.
Burris, L., Steindler, M., and Miller, W. (1984) Proceeding of the International Topical Meeting Fuel Reprocessing and Waste Management, vol. 2, pp. 2–257.
Burris, L., Steunenberg, R.K., and Miller, W.E. (1986) Proceedings, Annual AIChE Meeting, vol. 83, pp. 135–142.
Cahalan, J.E., Sevy, R.H., and Su, S.F. (1985) Proceeding of the International Topical Meeting Fast Reactor Safety, vol. 1, p. 29.
Campbell, D.R. and Huntington, H.B. (1969) *Phys. Rev.*, **179**, 601–612.
Chang, Y.I. (1989) *Nucl. Technol.*, **88**, 129.
Chang, Y.I., Finck, P.J., and Grandy, C. (2006) Report ANL-ABR-1, Argonne National Laboratory.
Claudson, T.T., Geering, G.T., Goffard, J.W., and Minor, J.E. (1959) *A Symposium on Effects of Irradiation on Fuel and Fuel Elements: Nuclear Metallurgy*. Chicago, TMS-AIME, p. VI.
Clough, D.J. (1970) Proceeding of the ANS/ENS Meeting Fast Reactor Fuel and Fuel Elements, Karlsruhe, Germany, pp. 321–341.
Clough, D.J. (1977) *J. Nucl. Mater.*, **65**, 24.
D'Amico, J.F. and Huntington, H.B. (1969) *J. Phys. Chem. Solids*, **30**, 1607–1621.
Dienst, W. (1977) *J. Nucl. Mater.*, **65**, 1.
Di Novi, R.A. (1972) Report ANL-7889, Argonne National Laboratory.
Enderby, J.A. (1956) Report ICR-R/R. 198, UK Atomic Energy Authority.
Englander, M. and Montpreville, C.T. (1968) Proceedings of the 11th Colloque de Metallurgie, CEN, Saclay, France.
Frost, B.R.T., Mardon, P.G., and Russell, L.E. (1962) Proceedings of the Plutonium as a Power Reactor Fuel. Report HW 7500, 7, Hanford Works.
Gan, J., Keiser, D.D., Jr,, Wachs, D.M., Robinson, A.B., Miller, B.D., and Allen, T.R. (2010) *J. Nucl. Mater.*, 396, 234–239.
Gittus, J.H. (1963) *Uranium*, Butterworths, London.
Greenwood, G. W. (1961), *J. Nucl. Mater.* **6**, 1 26–34.
Harrington, C.D. and Ruehle, A.E. (1958) *Uranium Production Technology*, sponsored by the U.S. Atomic Energy Commission, D. Van Nostrand, Princeton, NJ.
Hehenkamp, Th. (1977) Electro- and thermotransport in metals and alloys. AIME Symposium, Niagara Falls, New York, September 1976.
Henry, K.J. and Edwards, A.G. (1966) *Fast Breeder Reactors*, Pergamon Press, Oxford, pp. 153–170.
Hesketh, M. (1968) Discussion in Paper: M. Englander, C.T. Montpreville, 11th Colloque de Metallurgie, Creep, June 1967, Centre d'Etudes Nucleaires de Saclay, p. 28.
Hofman, G.L. (1980) *Nucl. Technol.*, **47**, 7.
Hofman, G.L., Beck, W.N., Strain, R.V., Hayner, G.O., and Walter, C.M. (1976) Report ANL-8119, Argonne National Laboratory.
Hofman, G.L., Hins, A.C., Porter, D.L., Leibowitz, L., and Wood, E.L. (1986) Proceeding of the Conference Reliable Fuels for Liquid Metal Reactors, ANL-AIME, Tucson, AZ.
Hofman, G.L., Pahl, R.G., Lahm, C.E., and Porter, D.L. (1990), *Met. Trans. A*., **21A**, 517.
Horak, J.A., Kittel, J.H., and Dunworth, R.J. (1962) Report ANL-6429, Argonne National Laboratory.
Hudson, B. (1964) *Philos. Mag.*, **10**, 949.
Jepson, M.D. and Slattery, C.F. (1961) British Patent 063 492, 1958–1961.
Johnson, P.B., Gilberd, P.W., Morrison, Y., and Varoy, C.R. (1997) *Nucl. Instrum. Methods*, **B127**, 734.
Kim, Y.S., Hofman, G.L., Cheon, J.S., Robinson, A.B., and Wachs, D.M. (2012) Proceedings of the International Meeting, RERTR 2012, Warsaw, Poland, October 14–17.
Kittel, J.H. (1949) Report ANL-4937, Argonne National Laboratory.
Kittel, J.H. (1977) Report ANL-AFP-38, Argonne National Laboratory.
Kittel, J.H., Bierlein, T.K., Hayward, B.R., and Thurber, W.C. (1964) Proceedings of the 3rd International Conference, Peaceful Use of Atomic Energy, vol. 8/39-9/9, p. 227.
Kittel, J.H. and Horak, J.A. (1961) Report ANL-6516, Argonne National Laboratory, pp. 139–141.
Kittel, J.H. and Paine, S.H. (1958) Proceeding of the 2nd International Conference, Peaceful Uses of Atomic Energy, Geneva, Switzerland, vol. 5, pp. 500–509.
Kobayashi, T., Kinoshita, M., and Hattori, S. (1990) *Nucl. Technol.*, 80, 143.

Kramer, J.M. and Bauer, T.H. (1990) Proceedings of the International Conference on Fast Reactor Safety, p. 145.

Kryger, B. (1969) Contribution à Letude du Degagement Des Gaz De Fission Dans Le Comestible Nucleares Matalliques, Rapport CEA-R-3888.

Kulcinski, G.L., Leggett, R.D., Hann, C.R., and Mastel, B. (1969) *J. Nucl. Mater.*, **3**, 30.

Leggett, R.D., Bierlein, T.K., and Mastel, B. (1967) *Radiation Effects, AIME Symposium, Asheville (NC), September 1965*, Gordon and Breach, New York, p. 303.

Leggett, R.D., Hann, C.R., Mastel, B., and Mereka, K.R. (1966) Report BNWL-207, Battelle Northwest.

Leggett, R.D., Mastel, B., and Bierlein, T.K. (1963) Report HW-79559, Hanford Laboratories.

Lehmann, J., Blanchard, P., Paoli, P., Baron, J.L., and Azam, N. (1969) *Proceedings of the Symposium Radiation Damage in Reactor Materials*, IAEA, Vienna.

Lemoine, P. and Wachs, D.M. (2007) International Conference On Research Reactors, Sydney, Australia, November 2007, IAEA-CN - 156.

Leteurtre, J. (1969) Rapport CEA, R-3607, pp. 76–78.

Liu, Y., Tsai, H., Donahue, D., Pushis, D., Savoie, F., Holland, J., Wright, A., August, C., Bailey, J., and Patterson, D. (1990) Proceedings of the International Conference Fast Reactor Safety, p. 491.

Loomis, B.A. and Gerber, S.B. (1968) *Philos. Mag.*, **18**, 539.

Makin, M.J., Chatwin, W.H., Evans, J.H., Hudson, B., and Hyam, E.D. (1962) Institute of Metals Symposium on Uranium and Graphite, London, UK, Paper No. 7.

Marchaterre, J.F., Cahalan, J.E., Sevy, R.H., and Wright, A.E. (1985) Proceeding of the ASME Winter Meeting, ASME No. 82-WA/HT-37.

Marchaterre, J.F., Sevy, R.H., and Cahalan, J.E. (1986) Proceedings of the ASME Winter Meeting, ASME No. 86-WA/NE-14.

McDonell, W.R. (1965) *Nucleonics*, **23** (10), 72.

McDonell, W.R. (1973) *Proceedings of the Physical Metallurgy of Reactor Fuel Elements*, Berkeley Nuclear Laboratory, Gloucestershire.

McDonell, W.R. and Angerman, C.L. (1965) in *Proceedings of the AIME Conference on Radiation Effects, Asheville* (ed. W.F. Sheely), Gordon and Breach, New York, p. 411.

Merten, U., Bokros, J.C., Couggisberg, D.B., and Hatcher, A.P. (1963) *J. Nucl. Mater.*, **10** (3), 201.

Mikailoff, H. (1964) Quelques Aspects du Gonflement En Pile Des Materiaux Fissile, Rapport CEA-R2601.

Mohr, D., Chang, L.K., Feldman, E.E., Betten, P.R., and Planchon, H.P. (1987) *Nucl. Eng. Des.*, **101**, 11.

Monson, H.O. (1967) *Fast Breeder Reactors*, Pergamon Press, Oxford, pp. 135-152.

Murphy, W.F., Beck, W.N., Brown, F.L., Koprowski, B.J., and Neimark, L.A. (1969) Report ANL-7602, Argonne National Laboratory.

Mustelier, J.P. (1962) Symposium, Effects of Irradiation on Solids and Materials for Reactors, Venice, Italy.

O'Boyle, D.R. and Dwight, A.E. (1970) *Plutonium 1970 and Other Actinides Nuclear Metallurgy*, vol. 17, AIME.

Paine, S.H. and Kittel, J.H. (1955) Proceeding of the 1st International Conference on Peaceful Uses of Atomic Energy, vol. 7, p. 517.

Planchon, H.P., Sackett, J.I., Golden, G.H., and Sevy, R.H. (1987) *Nucl. Eng. Des.*, **101**, 75.

Porter, D.L., Lahm, C.E., and Pahl, R.G. (1990) *Met. Trans. A*, **21A**, 1871.

Pugh, S.F. (1955) Proceeding of the 1st International Conference on Peaceful Uses of Atomic Energy, vol. 7, p. 441.

Pugh, S.F. (1961) *The Metal Plutonium*, Chapter XXXI, University of Chicago Press, Chicago.

Roberts, A.C. and Cottrell, A.H. (1956) *Philos. Mag.*, **1**, 711–717.

Rough, F.A. and Bauer, A.A. (1958) Report BMI-1300, Battelle Memorial Institute.

Shewmon, P.G. (1958) *TMS-AIME*, **212**, 642–645.

Solomon, A.A. (1973) *J. Am. Ceram. Soc.*, **56**, 164.

Thomas, D.E., Fillnow, R.H. Goldman, K.M., Hino, J., Van Thyne, R.J., Holtz, F.C., and McPherson, D.J. (1958) Proceedings of the 2nd United Nations International Conference, Peaceful Uses of Atomic Energy, Geneva, Switzerland, vol. 5, No. 6.0.

Till, C.E. and Chang, Y.I. (1988) *Adv. Nucl. Sci. Technol.*, **20** 127.

Tsai, H. (1990) Proceedings of the International Conference Fast Reactor Safety, Snowbird (UT), August 12–16, p. 257.

Tsai, H. (1991) Proceedings of the International Conference Fast Reactors and Related Fuel Cycles, Kyoto, Japan.
Van Loo, F.J.J., Van Beak, J.A., Bastin, C.F., and Metselaar, R. (1984) *Diffusion in Solids, Symposium*, TMS-AIME, Detroit, MI.
Wade, D.C. and Chang, Y.I. (1988) *Nucl. Sci. Eng.*, **100**, 507.
Walters, L.C., Seidel, B.R., and Kittel, J.H. (1984) *Nucl. Technol.*, **65**, 179.
Wever, H. (1973) *Elektro- und Thermotransport in Metallen*, J. A. Barth-Verlag, Leipzig.
White, R.J. (1999) The Re-irradiation of MIMAS-MOX Fuel. Project Report IFA-629.1, HWR-586, Halden Reactor.
Zaimovsky, A.S. (1958) Proceedings of the 2nd International Conference, Peaceful Uses of Atomic Energy, vol. 5, p. 566, Geneva.
Zegler, S.T. (1967) ANL-7417, Argonne National Laboratory.
Zegler, S.T. and Walter, C.M. (1967) Plutonium Fuels Technology, AIME Symposium 13, Scottsdale, AZ, p. 335.
Zeisser, P., Maraniello, G., and Combette, P. (1977) *J. Nucl. Mater.*, **65**, 48.

Further Reading

Burke, J.J., Colling, D.A., Gorium, A.E., and Greenspan, J. (eds) (1962) *Physical Metallurgy of Uranium Alloys; Proceedings of the Third Army Materials Technology Conference. Brook Hill Publishing, Chestnut Hill, MA.*
Feldman, E.E., Mohr, D., Chang, L.K., Planchon, H.P., Dean, E.M., and Betten, P.R. (1987) *Nucl. Eng. Des.*, **101**, 57.
Frost, B.R.T. (1982) *Nuclear Fuel Elements (Design, Fabrication and Performance).* Pergamon Press, Oxford, New York.
Ishida, M. (1990) *Nucl. Technol.*, 89, 89.
Konobeevsky, S.T., Dubrovin, K.P., Levitsky, B.M., Pantaleev, L.D., and Pravdyuk, N.F. (1958) Proceedings of the 2nd International Conference, Peaceful Uses of Atomic Energy, vol. 5, pp. 574–586.
Lehmann, J., Paoli, P., and Azam, N. (1968) *J. Nucl. Mater.*, **27**, 285.
Leteutre, J. and Quere, Y. (1967) Irradiation effects in fissile materials, in: *Defects in Crystalline Solids*, vol. 6 (eds S. Amelinckx, R. Gevers, and J. Nihoul), North-Holland, American Elsevier, Amsterdam, New York.
Matzke, H.J. (1986) *Science of Advanced LMFBR Fuels*, North-Holland, Amsterdam.
Kaufmann, A.R. (ed.) (1964) *Nuclear Reactor Fuel Elements: Metallurgy and Fabrication* (prepared under the auspices of the Division of Technical Information, United Atomic Energy Commission), Wiley-Interscience, New York, pp. 293–361.
Pahl, R.G., Porter, D.L., Lahm, C.E., and Hofman, G.L. (1990a) *Met. Trans. A.*, **21 A**, 1963.
Pahl, R.G., Wisner, R., Billone, M., and Hofman, G.L. (1990b) Proceedings of the International Conference on Fast Reactor Safety, Snowbird, UT, August 12–16, p. 129.
Seidel, B.R. and Einzinger, R.E. (1977) *Radiation Effects in Breeder Reactor Structural Materials*, Metallurgical Society of AIME, p. 139.
Seidel, B.R., Porter, D.L., Walters, L.C., and Hofman, G.L. (1986a) Proceedings of the International Conference on Reliable Fuels for Liquid Metal Reactors, Tucson, AZ, September 7–11, pp. 2–106.
Seidel, B.R., Batté, G.L., Lahm, C.E., Fryer, R.M., Koenig, J.F., and Hofman, G. L. (1986b) Proceedings of the International Conference on Reliable Fuels for Liquid Metal Reactors, Tucson, AZ, September 7–11, pp. 6–48.
Tracy, D.B., Henslee, S.P., Dodds, N.E., and Longua, K.J. (1989) *Trans. Am. Nucl. Soc.*, **60**, 314.
Walter, C.M., Golden, G.H., and Olson, N.J. (1975) U–Pu–Zr Metal Alloy – A potential fuel for LMFBR ANL, Report ANL-76-28, Argonne National Laboratory.
Walter, C.M., Olson, N.J., and Hofman, G.L. (1973) *Nucl. Met.*, **19**, 181.